

# Capacity Optimality of OAMP: Beyond IID Sensing Matrices and Gaussian Signaling

Lei Liu, *Member, IEEE*, Shansuo Liang, and Li Ping, *Fellow, IEEE*

## Abstract

This paper studies a large unitarily invariant system (LUIS) involving a unitarily invariant sensing matrix, an arbitrary signal distribution, and forward error control (FEC) coding. We develop a universal Gram-Schmidt orthogonalization for orthogonal approximate message passing (OAMP). Numerous area properties are established based on the state evolution and minimum mean squared error (MMSE) property of OAMP in an un-coded LUIS. As a byproduct, we provide an alternative derivation for the constrained capacity of a LUIS. Under the assumption that the state evolution for OAMP is correct for the coded system, the achievable rate of OAMP is analyzed. We prove that OAMP achieves the constrained capacity of the LUIS with an arbitrary signal distribution provided that a matching condition is satisfied. Meanwhile, we elaborate a capacity-achieving coding principle for LUIS, based on which irregular low-density parity-check (LDPC) codes are optimized for binary signaling in the numerical results. We show that OAMP with the optimized codes has significant performance improvement over the un-optimized ones and the well-known Turbo linear MMSE algorithm. For quadrature phase-shift keying (QPSK) modulation, capacity-approaching bit error rate (BER) performances are observed under various channel conditions.

## Index Terms

Orthogonal approximate message passing (OAMP), large unitarily invariant system, arbitrary input distributions, area properties, channel capacity, coding principle

## I. INTRODUCTION

### A. Receiver Optimality in Un-coded and Coded Linear Systems

Consider estimating  $\mathbf{x} = \{x_i\} \in \mathbb{C}^N$  from an observation  $\mathbf{y} \in \mathbb{C}^M$  in a linear system

$$\mathbf{y} = \mathbf{A}\mathbf{x} + \mathbf{n}, \quad (1a)$$

Lei Liu was with the Department of Electronic Engineering, City University of Hong Kong (CityU), Hong Kong, SAR, China, and is currently with the School of Information Science, Japan Institute of Science and Technology (JAIST), Ishikawa 923-1292, Japan (e-mail: leiliu@jaist.ac.jp).

Shansuo Liang and Li Ping are with the Department of Electronic Engineering, City University of Hong Kong, Hong Kong, SAR, China (e-mail: ssliang3-c@my.cityu.edu.hk, eiping@cityu.edu.hk).

where  $\mathbf{n} \in \mathbb{C}^M$  contains independently and identically distributed (IID) Gaussian noise samples. For convenience, we refer to  $\mathbf{A} \in \mathbb{C}^{M \times N}$  as a sensing matrix. We assume that  $\{x_i\}$  follow an a priori distribution

$$x_i \sim P_X(x_i), \quad \forall i. \quad (1b)$$

Furthermore, we assume that  $\mathbf{x}$  is generated by a forward error control (FEC) code that includes un-coded  $\mathbf{x}$  as a special trivial case.

A wide range of communication applications can be modeled by (1). A classic one is a multiple-input multiple-output (MIMO) system where  $\mathbf{A}$  is a channel coefficient matrix [1], [2] and  $P_X(x_i)$  is determined by the signaling (i.e., modulation) method. Continuous Gaussian signaling, with which  $\{x_i\}$  are IID Gaussian, is often assumed in information theoretical studies but, due to implementation concerns, all practically used signaling methods are discrete such as the quadrature phase-shift keying (QPSK) uniformly distributed on  $\{\pm \frac{1}{\sqrt{2}}, \pm \frac{1}{\sqrt{2}}i\}$ .

A more recent application of (1) is the so-called massive-access scheme where  $\mathbf{A}$  consists of pilot signals and  $P_X(x_i)$  is jointly determined by channel coefficients and user activity [3], [4]. In this case, a common assumption of  $P_X(x_i)$  is Bernoulli-Gaussian that is continuous. Massive-access has attracted wide research interests for machine-type communications in the 5<sup>th</sup> and 6<sup>th</sup> generation (5G and 6G) cellular systems.

Two performance measures are commonly used for the system in (1), namely mean squared error (MSE) for an un-coded system and achievable rate for a FEC coded one. The optimal limits in these two cases are respectively given by minimum MSE (MMSE) and information theoretic capacity. For convenience, we will say that a receiver is

- MMSE-optimal if its MSE achieves MMSE when  $\mathbf{x}$  is un-coded, or
- capacity-optimal if its achievable rate reaches mutual information  $I(\mathbf{x}; \mathbf{y})$  when  $\mathbf{x}$  is coded.

Optimal receivers under both measures generally have prohibitively high complexity [5], [6] except for a few cases. Some of such special cases are listed below.

- The classic linear MMSE (LMMSE) detector is optimal when (1) is un-coded with IID Gaussian signaling [7].
- Some compressed-sensing algorithms are asymptotically (with  $N \rightarrow \infty$ ) MMSE-optimal when  $\mathbf{x}$  is un-coded and sparse<sup>1</sup>.
- When  $\mathbf{A}$  is diagonal, (1) is equivalent to a set of parallel single-input-single-output (SISO) sub-systems. Turbo [8], [9] or low-density parity-check (LDPC) [10], [11] codes are nearly capacity-optimal in this case.
- For Gaussian signaling, Turbo-type detection algorithms [12] are capacity-optimal using proper coding [13]–[15].

<sup>1</sup>  $\mathbf{A}$  or  $\mathbf{x}$  in (1) is sparse if its entries are dominated by zeros. Otherwise, they are dense.

For discrete signaling with dense  $\mathbf{A}$  and  $\mathbf{x}$ , however, detection methods with proven MMSE or capacity optimality and practical complexity remained a difficult issue until recently [16]–[20].

### B. AMP and Related Algorithms

Approximate message passing (AMP) represents a remarkable progress measured by both types of optimality with practical complexity. AMP employs a so-called Onsager term to regulate the correlation problem in iterative processing [21]. A distinguished feature of AMP is that its performance can be accurately analyzed by a state-evolution (SE) technique in an asymptotic case with  $M, N \rightarrow \infty$  with their ratio fixed [22]. Based on SE, the MMSE optimality AMP are proved in [16], [17]. The capacity optimality of AMP is proved in [20].

We will say that  $\mathbf{A}$  in (1) is IIDG when its entries are IID Gaussian. Good performance of AMP is guaranteed only when  $\mathbf{A}$  is IIDG. This IIDG restriction is relaxed in orthogonal AMP (OAMP) [23]–[25]. Let the singular value decomposition (SVD) of  $\mathbf{A}$  be

$$\mathbf{A} = \mathbf{U}^H \Sigma \mathbf{V}, \quad (2)$$

where  $\mathbf{U} \in \mathbb{C}^{M \times M}$  and  $\mathbf{V} \in \mathbb{C}^{N \times N}$  are unitary and  $\Sigma$  is an  $M \times N$  rectangular diagonal matrix. We will say that  $\mathbf{V}$  is Haar distributed if  $\mathbf{V}$  is uniformly distributed over all unitary matrices [26], [27]. We will say that  $\mathbf{A}$  is *right-unitarily invariant* if  $\mathbf{V}$  in (2) is Haar distributed. We will call (1) a large unitarily invariant system (Luis) when  $M \rightarrow \infty$ ,  $N \rightarrow \infty$  with their ratio fixed and  $\mathbf{V}$  is Haar distributed. The SE for OAMP is conjectured for Luis in [23] and rigorously proved in [28], [29]. The MMSE-optimality of OAMP in Luis is derived in [18], [19] under the assumption that the SE for OAMP is accurate. Recently, to avoid the high complexity LMMSE in OAMP, low-complexity convolutional AMP (CAMP) [30] and memory AMP (MAMP) [31] were proposed for Luis. Unitarily-invariant matrices form a larger set that includes IIDG matrices as a special case. Hence OAMP is applicable to a wider range of sensing matrices than AMP.

### C. Contributions of This Paper

In this paper, we prove the capacity-optimality of OAMP.

AMP-type algorithms, including OAMP, all involve iteration between two local processors such as linear estimator (LE)  $\gamma$  and non-linear estimator (NLE)  $\phi$  [21], [23], [28]. The performance of these two local processors can be respectively characterized by two transfer functions  $\gamma_{\text{SE}}$  and  $\phi_{\text{SE}}$  using the SE technique [22], [28], [29]. Detailed discussions on  $\gamma_{\text{SE}}$  and  $\phi_{\text{SE}}$  can be found in Subsection IV-A below, and also [22], [28], [29]. The convergence point of SE is a fixed point of  $\gamma_{\text{SE}}$  and  $\phi_{\text{SE}}$ .

Following [20], we call mutual information  $I(\mathbf{x}; \mathbf{y})$  the constrained capacity of the system in (1). In [20], we showed that the achievable rate of AMP is equal to an area determined

by  $\gamma_{\text{SE}}$  and  $\phi_{\text{SE}}$ . When the two local processors in AMP are MMSE-optimal, we can apply the celebrated I-MMSE theorem [20] to derive the achievable rate of AMP. We showed in [20] that this achievable rate equals the constrained capacity under a matching condition of the underlying FEC code. Thereby we proved the capacity-optimality of AMP. The assumption of MMSE-optimal NLE  $\phi$  is the key in the proof of capacity optimality of AMP [20].

Unfortunately, we cannot assume the local processors in OAMP are MMSE-optimal. This is due to the requirement of input-output error orthogonality on the local processors in OAMP. MMSE-optimal processors are generally not orthogonal, so the local processors in OAMP are generally not MMSE-optimal. This constitutes a main difficulty in extending the results on AMP in [20] to OAMP.

In this paper, we will overcome the difficulty using a Gram-Schmidt model of an orthogonal local processor. Based on this model, we establish a connection between an arbitrary local processor and an orthogonal one. This connection leads to an equivalent structure of OAMP such that the NLE  $\phi$  can be MMSE-optimal. Such local-optimality allows the use of the I-MMSE theorem to obtain the achievable rate of OAMP. We prove that this achievable rate is equal to the constrained capacity, which leads to the capacity-optimality of OAMP.

The proof of capacity-optimality of OAMP in this paper can also be extended to the vector AMP algorithm (VAMP) [28] due to the algorithmic equivalence between two algorithms. Such equivalence is noted in [30]–[32]. Furthermore, using the Gram-Schmidt model, we will discuss the similarity and difference between OAMP and the expectation propagation (EP) algorithm. We will show OAMP and EP are equivalent when OAMP is designed using MMSE-optimal prototypes. This equivalence implies that EP is also capacity-optimal under proper FEC coding.

OAMP is being extensively investigated in many emerging applications including MIMO channel estimation and massive access [32]–[36] since it is not restricted to systems with Gaussian signaling, sparsity and IIDG sensing matrices. Most exiting works on OAMP are for un-coded case. The findings in this paper provides an optimization technique for coded cases.

#### D. Notations

Boldface lowercase letters represent vectors and boldface uppercase symbols denote matrices. We say that  $x = x_{\text{Re}} + ix_{\text{Im}}$  is circularly-symmetric complex Gaussian (CSCG) if  $x_{\text{Re}}$  and  $x_{\text{Im}}$  are two independent Gaussian distributed random variables with  $\text{E}\{x_{\text{Re}}\} = \text{E}\{x_{\text{Im}}\} = 0$  and  $\text{Var}\{x_{\text{Re}}\} = \text{Var}\{x_{\text{Im}}\}$ . We define  $\text{Var}\{x\} \equiv \text{Var}\{x_{\text{Re}}\} + \text{Var}\{x_{\text{Im}}\}$ . Denote  $I(\mathbf{x}; \mathbf{y})$  for the mutual information between  $\mathbf{x}$  and  $\mathbf{y}$ ,  $\mathbf{I}$  for the identity matrix with a proper size,  $\mathbf{a}^H$  for the conjugate transpose of  $\mathbf{a}$ ,  $\|\mathbf{a}\|$  for the  $\ell_2$ -norm of the vector  $\mathbf{a}$ ,  $\det(\mathbf{A})$  for the determinant of  $\mathbf{A}$ ,  $\text{tr}(\mathbf{A})$  for the trace of  $\mathbf{A}$ ,  $A_{ij}$  for the  $i$ th-row and  $j$ th-column element of  $\mathbf{A}$ ,  $\mathcal{CN}(\boldsymbol{\mu}, \boldsymbol{\Sigma})$  for the CSCG distribution with mean  $\boldsymbol{\mu}$  and covariance  $\boldsymbol{\Sigma}$ ,  $\text{E}\{\cdot\}$  for the expectation operation over all

random variables involved in the brackets, unless otherwise specified.  $E\{a|b\}$  for the expectation of  $a$  conditional on  $b$ ,  $\text{var}\{a\}$  for  $E\{\|a - E\{a\}\|^2\}$ ,  $\text{mmse}\{a|b\}$  for  $E\{\|a - E\{a|b\}\|^2|b\}$ ,  $\langle \mathbf{x} \rangle = \sum_{i=1}^N x_i/N$ , and  $\eta'(r) = \frac{\partial}{\partial r}\eta(r)$ .

Throughout this paper, unless stated otherwise, we will assume that (i) the length of a vector is  $N$  and (ii)  $\mathbf{x}$  is normalized, i.e.,  $\frac{1}{N}E\{\|\mathbf{x}\|^2\} = 1$ .

Capacity is defined by default as the maximum mutual information over all possible choices of input distribution. A constrained capacity is defined as the mutual information under a fixed input distribution  $\mathbf{x} \sim P_X(\mathbf{x})$ . For the systems considered in this paper, capacity is always achieved by Gaussian signaling. Hence sometimes we will call it “Gaussian capacity”. For simplicity, we will call the constrained capacity given  $P_X(\mathbf{x})$  “capacity” if it is clear by context.

### E. Paper Outline

This paper is organized as follows. Section II gives the system model and preliminaries. Section III introduces an OAMP based on a universal Gram-Schmidt orthogonalization. Section IV derives the state evolution of OAMP and area properties. Achievable rates of OAMP in the coded LUIS are established in Section V. Numerical results are shown in Section VI.

## II. SYSTEM MODEL AND PRELIMINARIES

A large unitarily invariant system (LUIS) in (1) consists of a linear constraint  $\Gamma$  and a non-linear constraint  $\Phi$ :

$$\text{Linear constraint } \Gamma : \mathbf{y} = \mathbf{A}\mathbf{x} + \mathbf{n}, \quad (3a)$$

$$\text{Non-linear constraint } \Phi : \mathbf{x} \sim P_X(\mathbf{x}), \quad (3b)$$

where  $\mathbf{y} \in \mathbb{C}^{M \times 1}$  is a vector of observations,  $\mathbf{A} \in \mathbb{C}^{M \times N}$  a *right-unitarily invariant* measurement matrix (see I-B) and  $\mathbf{n} \sim \mathcal{CN}(\mathbf{0}, \sigma^2 \mathbf{I}_M)$  a vector of additive Gaussian noise samples. Since  $\mathbf{x}$  is normalized, the transmit SNR is defined as  $\text{snr} = \sigma^{-2}$ . We consider a large-scale LUIS that  $M, N \rightarrow \infty$  and a fixed  $\beta = N/M$ .  $\mathbf{A}$  is known at the receiver, but unknown at the transmitter<sup>2</sup>. This assumption has been widely used in multiple-input-multiple-output (MIMO) [32] and multi-user MIMO systems [14]. Fig. 1 shows a block diagram of LUIS.

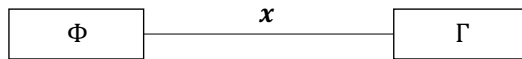


Fig. 1. Graphical illustration for a LUIS with two constraints  $\Gamma$  and  $\Phi$ .

<sup>2</sup>If  $\mathbf{A}$  is also known at the transmitter, then the LUIS in (1) can be converted to a set of parallel SISO-AWGN channels using singular value decomposition (SVD). Then, the well-known water filling technique is capacity approaching.

### A. Un-coded LUIS

For an un-coded LUIS, the non-linear constraint in (3b) is rewritten to a constellation constraint:

$$\text{Constellation constraint } \Phi_S : \quad x_i \sim P_X(x), \quad \forall i. \quad (4)$$

That is, the entries of  $\mathbf{x}$  are IID with distribution  $P_X(x)$ .

In the un-coded LUIS, mean squared error (MSE) is commonly used for performance measurement. If  $P_X(x)$  is a Gaussian distribution, the optimal solution is the standard linear minimum MSE (MMSE) estimate. For non-Gaussian distribution  $P_X(x)$ , finding the optimal solution is generally NP hard [5], [6].

*Minimum Mean Square Error (MMSE):* Our aim is to find an MMSE estimation of  $\mathbf{x}$ . That is, the estimation MSE converges to

$$\text{mmse}\{\mathbf{x}|\mathbf{y}, \mathbf{A}, \Gamma, \Phi\} \equiv \frac{1}{N} \mathbb{E}\{\|\hat{\mathbf{x}}_{\text{post}} - \mathbf{x}\|^2\}, \quad (5)$$

where  $\hat{\mathbf{x}}_{\text{post}} = \mathbb{E}\{\mathbf{x}|\mathbf{y}, \mathbf{A}, \Gamma, \Phi\}$  is the *a-posteriori* mean of  $\mathbf{x}$ .

### B. Coded LUIS

In the un-coded LUIS, an error-free estimation can not be guaranteed. To ensure an error-free estimation, we consider the LUIS with forward error control (FEC) coding. For a coded LUIS, the non-linear constraint in (3b) is rewritten to a code constraint:

$$\text{Code constraint } \Phi_C : \quad \mathbf{x} \in \mathcal{C} \quad \text{and} \quad x_i \sim P_X(x), \quad \forall i, \quad (6)$$

where the entries of  $\mathbf{x}$  have the identical distribution  $P_X(x)$ .

In a coded LUIS, achievable rate is commonly used for performance metrics. For a specific receiver, the code rate  $R_C$  of  $\mathcal{C}$  is an achievable rate, if its estimation of  $\mathbf{x}$  under code constraint  $\mathcal{C}$  is error-free, i.e.,  $\text{mmse}\{\mathbf{x}|\mathbf{y}, \mathbf{A}, \Gamma, \Phi_C\} \rightarrow 0$ . A natural upper bound of achievable rate is the constrained capacity of LUIS, i.e., the mutual information under a fixed input distribution  $x \sim P_X(x)$ :

$$R_C \leq C_{\text{LUIS}} = I(\mathbf{x}; \mathbf{y}). \quad (7)$$

*Capacity Optimality:* Our aim is to find a coding scheme and a receiver with practical complexity such that the achievable rate approaches the constrained capacity of LUIS, i.e.,  $R_C \rightarrow C_{\text{LUIS}}$ .

For Gaussian signaling, the constrained capacity of LUIS is the well-known Gaussian capacity [2] below.

*Lemma 1:* The Gaussian capacity of a LUIS with  $\mathbf{x} \sim \mathcal{CN}(\mathbf{0}, \mathbf{I})$  is given by

$$C_{\text{Gau-LUIS}}(\text{snr}) = \frac{1}{N} \log \det (\mathbf{I} + \text{snr} \mathbf{A}^H \mathbf{A}). \quad (8)$$

For arbitrary signal distributions (can be non-Gaussian), the constrained capacity of LUIS is not trivial and was recently solved in [18] as shown in the following lemma.

*Lemma 2:* Assume that  $\rho^*$  is the unique solution of  $\rho^* = \text{snr} \mathcal{R}_{\mathbf{R}}(-\text{snr} v^*)$  where  $v^* = \text{mmse}\{\mathbf{x}|\sqrt{\rho^*}\mathbf{x} + \mathbf{z}, \Phi\}$ . The constrained capacity<sup>3</sup> of a LUIS is

$$C_{\text{LUIS}}(\text{snr}) = \int_0^{v^* \text{snr}} \mathcal{R}_{\mathbf{R}}(-z) dz + I(x; \sqrt{\rho^*}x + z) - \rho^* v^*, \quad (9)$$

where  $z \sim \mathcal{CN}(0, 1)$ , and  $\mathcal{R}_{\mathbf{R}}(\cdot)$  is the *R-transform* of matrix  $\mathbf{R} = \mathbf{A}^H \mathbf{A}$  (see [27] for an introduction to this transform).

### C. I-MMSE Lemma and Code-Rate-MMSE Lemma

The connections between the MMSE, constrained capacity of LUIS and code rate are established in [37], [38]. They will be used in the achievable rate analysis of OAMP (see Section V) and an alternative proof of the constrained capacity of LUIS (see Appendix D).

A SISO-AWGN channel is defined as

$$\Gamma_{\text{SISO}} : y = \sqrt{\rho}x + z, \quad (10a)$$

$$\Phi_{\mathcal{S}} : x \sim p_X(x). \quad (10b)$$

where  $z \sim \mathcal{CN}(0, 1)$ , and  $\rho$  denotes the signal-to-noise-ratio (SNR).

The following lemma, proved in [37], establishes the connection between MMSE and the constrained capacity given  $p_X(x)$  for a SISO-AWGN channel.

*Lemma 3 (Scalar I-MMSE):* The capacity of a SISO-AWGN channel equals to the area under  $\hat{\phi}_{\text{SE}}^{\mathcal{S}}(\rho)$  from  $\rho = 0$  to  $\rho = \text{snr}$ , i.e.,

$$C_{\text{SISO}}(\text{snr}) = I(x; \sqrt{\text{snr}}x + z) = \int_0^{\text{snr}} \hat{\phi}_{\text{SE}}^{\mathcal{S}}(\rho) d\rho, \quad (11)$$

where  $\hat{\phi}_{\text{SE}}^{\mathcal{S}}(\rho) \equiv \text{mmse}(x|\sqrt{\rho}x + z, \Phi_{\mathcal{S}})$  is the MMSE of (10).

The following lemma, proved in [38], establishes the connection between MMSE and code rate given  $p_X(x)$ .

*Lemma 4 (Code-Rate-MMSE):* Consider a code constraint  $\Phi_{\mathcal{C}} : \mathbf{x} \in \mathcal{C}$ . Let the code length be  $N$  and code rate  $R_{\mathcal{C}}$ . Then the rate of  $\mathcal{C}$  is given by

$$R_{\mathcal{C}} = \int_0^{\infty} \hat{\phi}_{\text{SE}}^{\mathcal{C}}(\rho) d\rho = K/N, \quad (12)$$

where  $\hat{\phi}_{\text{SE}}^{\mathcal{C}}(\rho) \equiv \frac{1}{N} \text{mmse}(\mathbf{x}|\sqrt{\rho}\mathbf{x} + \mathbf{z}, \Phi_{\mathcal{C}})$  is obtained by *a-posteriori* probability (APP) decoding.

<sup>3</sup>The capacity in (9) is equivalent to that in [18]. Some notes are as follows. First,  $\rho$ ,  $\text{snr}$  and  $v^*$  in (9) correspond to  $r$ ,  $\lambda$  and  $E$  in [18] respectively. Second, the factor  $1/2$  for a real LUIS in [18] is removed in (9) for a complex LUIS.

The connection between the measurement MMSE and the constrained capacity of a LUIS is given by the following lemma proven in [37].

*Lemma 5 (Vector I-MMSE [37]):* Consider a system  $\mathbf{y} = \sqrt{snr}\mathbf{Ax} + \mathbf{z}$  where  $\mathbf{x} \sim P_x$  and  $\mathbf{z} \sim \mathcal{CN}(\mathbf{0}, \mathbf{I})$ , and let  $\hat{\mathbf{x}}_{\text{post}} = \mathbb{E}\{\mathbf{x}|\mathbf{y}, \mathbf{x} \sim P_x\}$  be the *a-posteriori* mean of the un-coded  $\mathbf{x}$  given  $\mathbf{y}$  and  $\mathbf{x} \sim P_x$ . Then, the constrained capacity of this system is given by

$$C_{\text{LUIS}} = \frac{1}{N} I(\mathbf{x}; \sqrt{snr}\mathbf{Ax} + \mathbf{z}) = \int_0^{snr} \mathcal{M}_{Ax}(\rho) d\rho, \quad (13)$$

where  $\mathcal{M}_{Ax}(\rho) \equiv \frac{1}{N} \mathbb{E}\{\|\mathbf{Ax} - \mathbf{A}\hat{\mathbf{x}}_{\text{post}}\|^2\}$  is referred as the measurement MMSE of  $\mathbf{Ax}$ .

The MMSE optimality of OAMP was established in [18], [19]. Lemma 4 and Lemma 5 show the connection between the MMSE and constrained capacity of LUIS. These provide some hints of the potential capacity optimality of OAMP. However, how to design a coding scheme for OAMP to achieve the constrained capacity of LUIS is still an open issue. In this paper, we will prove the capacity optimality of OAMP based on a matching principle.

### III. ORTHOGONAL APPROXIMATE MESSAGE PASSING (OAMP)

OAMP is consisted of two orthogonal estimators. Specific forms of orthogonal estimators were first given in [23]. In this section, we will propose a kind of universal orthogonal estimators by Gram-Schmidt orthogonalization (GSO), which include the de-correlated linear estimator [23], divergence-free (e.g. differential-based) estimator [21], [23], integral-based orthogonal estimator [39], and expectation propagation (EP) [40]–[42] as special instances.

#### A. Gram-Schmidt (GS) Model

Let  $\hat{\mathbf{x}}$  be an arbitrary observation of  $\mathbf{x}$ . We generate a new vector  $\xi = \hat{\mathbf{x}} - \alpha\mathbf{x}$  using Gram-Schmidt orthogonalization [43], where

$$\alpha = \frac{1}{N} \mathbb{E}\{\hat{\mathbf{x}}^H \mathbf{x}\} \quad (14)$$

is a scalar. We will call (15) below the Gram-Schmidt (GS) model of  $\hat{\mathbf{x}}$  with respect to  $\mathbf{x}$ :

$$\hat{\mathbf{x}} = \alpha\mathbf{x} + \xi. \quad (15)$$

We treat  $\xi$  as an error term, referred to as the GS error below. Its average entry-wise power is

$$v = \frac{1}{N} \mathbb{E}\{\|\xi\|^2\} = \frac{1}{N} \mathbb{E}\{\xi^H \xi\}. \quad (16)$$

It can be verified that  $\xi$  is orthogonal to  $\mathbf{x}$ , i.e.

$$\mathbb{E}\{\mathbf{x}^H \xi\} = 0. \quad (17)$$

The error term  $\xi$  in (15) is different from the common definition of an error  $\hat{x} - x$ . For convenience, in the following, we will call  $\xi$  the GS error of  $\hat{x}$ . We will call  $\alpha$  and  $v$  GS parameters. The following lemma follows (15) directly.

*Lemma 6:* Assume that the distribution of  $x$  is given and  $\xi$  consists of IIDG entries with zero mean. Then the distribution of  $\hat{x}$  in (15) is completely specified by the GS parameters ( $\alpha$  and  $v$ ) of  $\hat{x}$ .

### B. Orthogonal Local Estimators

1) *Orthogonal Estimator:* Consider an estimator of  $x$ :

$$x_{\text{out}} = f(x_{\text{in}}), \quad (18)$$

where the input and output messages can be expressed in their GS models:

$$x_{\text{in}} = \alpha_{\text{in}}x + \xi_{\text{in}}, \quad (19a)$$

$$x_{\text{out}} = \alpha_{\text{out}}x + \xi_{\text{out}}. \quad (19b)$$

*Definition 1 (Orthogonal Estimator):* We say that  $f(\cdot)$  is an orthogonal estimator if

$$E\{\xi_{\text{in}}^H \xi_{\text{out}}\} = E\{\xi_{\text{in}}^H f(x_{\text{in}})\} = 0. \quad (20)$$

2) *Arbitrary Prototype and GS Orthogonalization (GSO):* In this part, we discuss techniques to realize the orthogonality required in (20). Let  $\hat{f}(x_{\text{in}})$  be an arbitrary prototype. As shown in Fig. 2, we construct an orthogonal  $f(x_{\text{in}})$  as follows

$$x_{\text{out}} = f(x_{\text{in}}) = \hat{f}(x_{\text{in}}) - Bx_{\text{in}}. \quad (21)$$

Then we can rewrite the orthogonal requirement as

$$E\{\xi_{\text{in}}^H \xi_{\text{out}}\} \stackrel{(a)}{=} E\{\xi_{\text{in}}^H [\hat{f}(x_{\text{in}}) - \alpha_{\text{out}}x]\} \stackrel{(b)}{=} E\{\xi_{\text{in}}^H \hat{f}(x_{\text{in}})\} \stackrel{(c)}{=} E\{\xi_{\text{in}}^H [\hat{f}(x_{\text{in}}) - Bx_{\text{in}}]\} = 0, \quad (22)$$

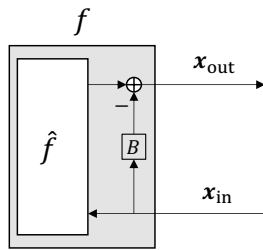


Fig. 2. Construction of an orthogonal estimator  $f(\cdot)$  via GSO based on an arbitrary prototype  $\hat{f}(\cdot)$ .

where equality (a) is due to  $\xi_{\text{out}} = f(\mathbf{x}_{\text{in}}) - \alpha_{\text{out}} \mathbf{x}$  (recalling from (17) for a GS model), (b) due to  $E\{\mathbf{x}^H \xi_{\text{in}}\} = 0$ , and (c) due to (21). Noting that  $E\{\xi_{\text{in}}^H \mathbf{x}_{\text{in}}\} = E\{\xi_{\text{in}}^H (\alpha_{\text{in}} \mathbf{x} + \xi_{\text{in}})\} = E\{\|\xi_{\text{in}}\|^2\}$  (recalling from (17) that  $E\{\mathbf{x}^H \xi_{\text{in}}\} = 0$  for a GS model), from (22) we have

$$B = E\{\xi_{\text{in}}^H \hat{f}(\mathbf{x}_{\text{in}})\} / E\{\|\xi_{\text{in}}\|^2\}. \quad (23)$$

3) *GSO Coefficient for Different Prototypes*: The key to GSO is to find  $B$ . Next, we show the forms of  $B$  for different prototypes  $\hat{f}(\cdot)$ .

(a) *B for Linear Prototypes*: Let  $\xi_{\text{in}}$  be IID with zero mean. For a linear prototype  $\hat{f}(\mathbf{x}_{\text{in}}) = \hat{\mathbf{W}} \mathbf{x}_{\text{in}} + \mathbf{b}$ , where  $\mathbf{b}$  is independent of  $\xi_{\text{in}}$ , then (23) reduces to [23]

$$B = \frac{1}{N} \text{tr}\{\hat{\mathbf{W}}\}. \quad (24)$$

Let  $\mathbf{W} = \hat{\mathbf{W}} - \frac{1}{N} \text{tr}\{\hat{\mathbf{W}}\} \mathbf{I}$ . For an orthogonal linear  $f$ , substituting (24) into  $f(\mathbf{x}_{\text{in}}) = \hat{f}(\mathbf{x}_{\text{in}}) - B \mathbf{x}_{\text{in}}$ , we have  $f(\mathbf{x}_{\text{in}}) = \mathbf{W} \mathbf{x}_{\text{in}} + \mathbf{b}$ , where  $\text{tr}\{\mathbf{W}\} = 0$ . On the other hand, if  $\text{tr}\{\mathbf{W}\} = 0$ , we have  $B = 0$  from (28) and also  $E\{\xi_{\text{in}}^H f(\mathbf{x}_{\text{in}})\} = 0$  from (23), i.e.,  $f(\mathbf{x}_{\text{in}}) = \mathbf{W} \mathbf{x}_{\text{in}} + \mathbf{b}$  is orthogonal. Thus, under the condition that  $\mathbf{x}$  is IID and  $\xi_{\text{in}}$  IID, a linear estimator  $f(\mathbf{x}_{\text{in}}) = \mathbf{W} \mathbf{x}_{\text{in}} + \mathbf{b}$  is orthogonal if and only if [23]

$$\text{tr}\{\mathbf{W}\} = 0. \quad (25)$$

(b) *B for General Prototypes*: In the following, we give the integral form and differential form of  $B$  for general prototypes.

- *Integral Form of B*: We consider a special case when  $\hat{f}$  is separable and integrable,  $\mathbf{x}$  IID and  $\xi_{\text{in}}$  IIDG (i.e.  $\xi_{\text{in}} \sim \mathcal{CN}(0, v_{\text{in}} \mathbf{I})$ ). Then (23) reduces to a integral form [39]:

$$B = \frac{\int_{-\infty}^{+\infty} \int_{-\infty}^{+\infty} \xi_{\text{in}} \hat{f}(\alpha_{\text{in}} x + \xi_{\text{in}}) p_{\xi_{\text{in}}}(\xi_{\text{in}}) p_x(x) d\xi_{\text{in}} dx}{\int_{-\infty}^{+\infty} \xi_{\text{in}}^2 p_{\xi_{\text{in}}}(\xi_{\text{in}}) d\xi_{\text{in}}}. \quad (26)$$

Assume that  $p_x(x)$  is known. Then (26) can be evaluated numerically. We may pre-calculate a table for  $B$  as a function of  $v_{\text{in}}$  off-line. Then cost is low for on-line processing. In some cases,  $\hat{f}$  may not be explicitly given. For example,  $\hat{f}$  can be a black-box type estimator in a software package. In this case, we can still generate  $B$ ,  $\alpha_{\text{out}}$  and  $v_{\text{out}}$  numerically by the Monte-Carlo method. The integral approach in (26) requires knowing  $p_x(x)$ . This condition is usually met in communication applications, but it may not be satisfied in some signal processing applications. The differential approach discussed next provides an alternative solution.

- *Differential Form of B*: The following is an alternative differential approach to calculate  $B$ , first introduced in [23] and inspired by [21]. From  $\xi_{\text{in}} \sim \mathcal{CN}(0, v_{\text{in}} \mathbf{I})$  and Stein's

Lemma [44], [45],

$$\frac{1}{N} \mathbb{E}\{\boldsymbol{\xi}_{\text{in}}^H \hat{f}(\mathbf{x}_{\text{in}})\} = v_{\text{in}} \mathbb{E}\{\partial \hat{f}(x_{\text{in}})/\partial x_{\text{in}}\}. \quad (27)$$

Hence, for  $N \rightarrow \infty$ , (23) can be rewritten as

$$B = \mathbb{E}\{\partial \hat{f}(x_{\text{in}})/\partial x_{\text{in}}\} \equiv \mathbb{E}\{\hat{f}'\}. \quad (28)$$

For an orthogonal  $f$ , substituting (28) into  $f(\mathbf{x}_{\text{in}}) = \hat{f}(\mathbf{x}_{\text{in}}) - B\mathbf{x}_{\text{in}}$ , the differential of  $f$  approaches zero. On the other hand, if the differential of  $f$  is zero, we have  $B = 0$  from (28) and also  $\mathbb{E}\{\boldsymbol{\xi}_{\text{in}}^H f(\mathbf{x}_{\text{in}})\} = 0$  from (23), i.e.,  $f$  is orthogonal. Thus, under the condition that  $\mathbf{x}$  is IID and  $\boldsymbol{\xi}_{\text{in}}$  IIDG, an estimator  $f$  is orthogonal if and only if

$$\mathbb{E}\{\partial f(x_{\text{in}})/\partial x_{\text{in}}\} = 0. \quad (29a)$$

Finally, when  $f$  is separable, (28) can be rewritten to

$$B \equiv \mathbb{E}\{\hat{f}'\} \approx \frac{1}{N} \sum_{i=1}^N \partial[\hat{f}(\mathbf{x}_{\text{in}})]_i / \partial[\mathbf{x}_{\text{in}}]_i. \quad (29b)$$

Eqn. (29b) does not require the distribution of  $\mathbf{x}$ , which makes it attractive in many signal processing problems. This advantage was first pointed out in [21].

(c) *B for Locally Optimal Prototypes*: When  $\hat{f}(\cdot)$  achieves MMSE,  $B$  in (23) can be calculated using the proposition below.

*Proposition 1*: Assume that  $\mathbf{x}_{\text{in}} = \mathbf{x} + \boldsymbol{\xi}_{\text{in}}$  and  $\hat{f}(\cdot)$  achieves local MMSE. Then

$$B = v_{\hat{f}}/v_{\text{in}}, \quad (30)$$

where  $v_{\hat{f}} \equiv \frac{1}{N} \mathbb{E}\{\|\hat{f}(\mathbf{x}_{\text{in}}) - \mathbf{x}\|^2\}$  and  $v_{\text{in}} \equiv \frac{1}{N} \mathbb{E}\{\|\boldsymbol{\xi}_{\text{in}}\|^2\}$ .

*Proof*: See Appendix A. ■

### C. Orthogonal AMP (OAMP)

We add an iteration index  $t$  to the estimates and formally define the iterative process in Fig. 3 as follows. Note that,  $\{\gamma_t\}$  and  $\{\phi_t\}$ , the messages  $\{\mathbf{x}_t^{\phi \rightarrow \gamma}, \hat{\mathbf{x}}_t^{\gamma \rightarrow \phi}\}$ ,  $\forall t$  in (31) are completely determined by initial values.

*Generic Iterative Process (GIP)*: Initializing from  $t = 0$  and  $\mathbf{x}_0^{\phi \rightarrow \gamma} = \mathbf{0}$ ,

$$\text{Linear estimator (LE)} : \quad \mathbf{x}_t^{\gamma \rightarrow \phi} = \gamma_t(\mathbf{x}_t^{\phi \rightarrow \gamma}), \quad (31a)$$

$$\text{Non-linear estimator (NLE)} : \quad \mathbf{x}_{t+1}^{\phi \rightarrow \gamma} = \phi_t(\mathbf{x}_t^{\gamma \rightarrow \phi}). \quad (31b)$$

In (31),  $\gamma_t(\cdot)$  and  $\phi_t(\cdot)$  respectively generate refined estimates of  $\mathbf{x}$ . Proper statistical models (e.g. GS models) of  $\mathbf{x}_t^{\phi \rightarrow \gamma}$  and  $\mathbf{x}_t^{\gamma \rightarrow \phi}$  are required for the design of  $\gamma_t(\cdot)$  and  $\phi_t(\cdot)$ , respectively.

Tracking such models is in general a prohibitively difficult task during iterative processing. This difficulty is resolved by OAMP using an orthogonal principle.

Let the messages in (31) be expressed in their GS models:

$$\mathbf{x}_t^{\phi \rightarrow \gamma} = \alpha_t^{\phi \rightarrow \gamma} \mathbf{x} + \boldsymbol{\xi}_t^{\phi \rightarrow \gamma}, \quad (32a)$$

$$\mathbf{x}_t^{\gamma \rightarrow \phi} = \alpha_t^{\gamma \rightarrow \phi} \mathbf{x} + \boldsymbol{\xi}_t^{\gamma \rightarrow \phi}. \quad (32b)$$

Let the average powers of the GS errors  $\boldsymbol{\xi}_t^{\phi \rightarrow \gamma}$  and  $\boldsymbol{\xi}_t^{\gamma \rightarrow \phi}$  be  $v^{\phi \rightarrow \gamma}$  and  $v_t^{\gamma \rightarrow \phi}$ , respectively.

*Orthogonal AMP (OAMP):* A GIP in (31) is said to be OAMP when the following orthogonal constraint holds for  $N \rightarrow \infty$ ,  $t \geq 0$ ,

$$\mathbb{E} \left\{ (\boldsymbol{\xi}_t^{\gamma \rightarrow \phi})^H \boldsymbol{\xi}_t^{\phi \rightarrow \gamma} \right\} = 0, \quad (33a)$$

$$\mathbb{E} \left\{ (\boldsymbol{\xi}_t^{\phi \rightarrow \gamma})^H \boldsymbol{\xi}_{t+1}^{\gamma \rightarrow \phi} \right\} = 0. \quad (33b)$$

That is,  $\gamma_t$  and  $\phi_t$  in (31) are orthogonal estimators.

The orthogonality in (33) is the key to solve the correlation problem. The GSO technique discussed in Section III-B can be used to construct the orthogonal estimators in OAMP. Let  $\hat{\gamma}_t$  and  $\hat{\phi}_t$  be the prototypes of LE and NLE, respectively. OAMP can be constructed as

$$\text{Orthogonal LE : } \mathbf{x}_t^{\gamma \rightarrow \phi} = \gamma_t(\mathbf{x}_t^{\phi \rightarrow \gamma}) = \hat{\gamma}_t(\mathbf{x}_t^{\phi \rightarrow \gamma}) - B_{\hat{\gamma}_t} \mathbf{x}_t^{\phi \rightarrow \gamma}, \quad (34a)$$

$$\text{Orthogonal NLE : } \mathbf{x}_{t+1}^{\phi \rightarrow \gamma} = \phi_t(\mathbf{x}_t^{\gamma \rightarrow \phi}) = \hat{\phi}_t(\mathbf{x}_t^{\gamma \rightarrow \phi}) - B_{\hat{\phi}_t} \mathbf{x}_t^{\gamma \rightarrow \phi}, \quad (34b)$$

where  $B_{\hat{\gamma}_t}$  and  $B_{\hat{\phi}_t}$  are GSO coefficients given in (23). In this paper, we consider locally optimal (e.g. MMSE) prototypes:

$$\text{LE : } \hat{\gamma}_t(\mathbf{x}_t^{\phi \rightarrow \gamma}) = \mathbb{E}\{\mathbf{x} | \mathbf{x}_t^{\phi \rightarrow \gamma}, \Gamma\}, \quad (35a)$$

$$\text{NLE : } \hat{\phi}_t(\mathbf{x}_t^{\gamma \rightarrow \phi}) = \mathbb{E}\{\mathbf{x} | \mathbf{x}_t^{\gamma \rightarrow \phi}, \Phi\}. \quad (35b)$$

Fig. 3 gives the block diagram of OAMP.

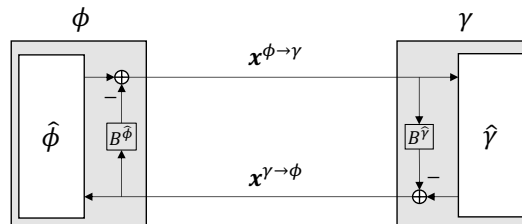


Fig. 3. Graphical illustration for OAMP receiver involving two local orthogonal estimators  $\gamma$  (for  $\Gamma$ ) and  $\phi$  (for  $\Phi$ ), which are constructed by GSO based on the prototypes  $\hat{\gamma}$  and  $\hat{\phi}$ , respectively.

*Equivalence Between OAMP and Expectation Propagation (EP):* Recall the EP updating rule [40]–[42]:

$$\mathbf{x}_{\text{out}} = f(\mathbf{x}_{\text{in}}) = \frac{1}{1 - v_{\hat{f}}/v_{\text{in}}} \left( \hat{f}(\mathbf{x}_{\text{in}}) - \frac{v_{\hat{f}}}{v_{\text{in}}} \mathbf{x}_{\text{in}} \right). \quad (36)$$

Clearly, (36) is equivalent to (21) with  $B$  given in (30). Therefore, EP and OAMP are equivalent when locally optimal prototypes are employed (see (35)). Otherwise, they are not. Therefore, GSO provides a new treatment for sub-optimal local estimators.

*Discussions:* The orthogonalization plays a central role in OAMP. It guarantees the error Gaussianity of an iterative process [23], [29]. Using the error Gaussianity, we can accurately characterize an iterative process via transfer functions. In fact, the performance of the orthogonalized estimator (e.g.  $\gamma_t$  and  $\phi_t$ ) is locally worse than the un-orthogonalized estimator (e.g.  $\hat{\gamma}_t$  and  $\hat{\phi}_t$ ). However, we will show that the orthogonalized iterative process converges to a globally (e.g. capacity/MMSE [18], [19] for coded/uncoded LUIS) optimal solution. On the contrary, if we directly use un-orthogonalized estimators for an iterative process, we may obtain better local transfer functions, but the iterative process cannot be characterized by the local transfer functions due to the correlation problem. As a result, its global performance is generally worse than the orthogonalized iterative process.

#### IV. STATE EVOLUTION OF OAMP AND AREA PROPERTIES

In this section, we introduce the state evolution and MMSE property of OAMP, based on which we will develop numerous area properties of LUIS.

##### A. State Evolution of OAMP in the Un-Coded LUIS

For simplicity of discussion, we rewrite the OAMP in (34) to

$$\mathbf{x}_t^{\eta \rightarrow \hat{\phi}} = \eta_t(\mathbf{x}_t^{\hat{\phi} \rightarrow \eta}), \quad (37a)$$

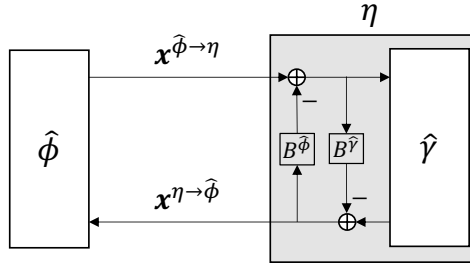
$$\mathbf{x}_{t+1}^{\hat{\phi} \rightarrow \eta} = \hat{\phi}_t(\mathbf{x}_t^{\eta \rightarrow \hat{\phi}}), \quad (37b)$$

where  $\eta_t$  includes  $\hat{\gamma}_t$  and the GSO operations. In fact,  $\eta_t$  contains a memory term  $\mathbf{x}_{t-1}^{\eta \rightarrow \hat{\phi}}$ , which is not explicitly shown in (37). Fig. 4(a) gives a graphical illustration of (37).

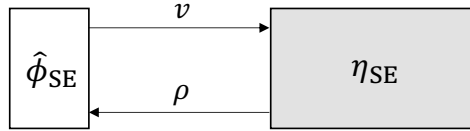
We define the true errors as:

$$\mathbf{e}_t^{\hat{\phi} \rightarrow \eta} \equiv \mathbf{x}_t^{\hat{\phi} \rightarrow \eta} - \mathbf{x}, \quad (38a)$$

$$\mathbf{e}_t^{\eta \rightarrow \hat{\phi}} \equiv \mathbf{x}_t^{\eta \rightarrow \hat{\phi}} - \mathbf{x}. \quad (38b)$$



(a) OAMP/EP receiver



(b) Transfer functions

Fig. 4. Graphical illustrations of (a) OAMP receiver and (b) the transfer functions.

Let  $v_t$  be the MSE of  $\mathbf{x}_t^{\hat{\phi} \rightarrow \eta}$  and  $\rho_t$  the signal to interference plus noise ratio (SINR) of  $\mathbf{x}_t^{\eta \rightarrow \hat{\phi}}$ :

$$v_t \equiv \frac{1}{N} \mathbb{E} \{ \| \mathbf{e}_t^{\hat{\phi} \rightarrow \eta} \|^2 \}, \quad (39a)$$

$$\rho_t \equiv \frac{1}{\frac{1}{N} \mathbb{E} \{ \| \mathbf{e}_t^{\eta \rightarrow \hat{\phi}} \|^2 \}}. \quad (39b)$$

The following lemma was proved in [28], [29] for OAMP in an un-coded LUIS with IID input  $\mathbf{x}$ , which ensures the correctness of the SE of OAMP.

*Lemma 7 (Asymptotic IIDG):* Let  $M, N \rightarrow \infty$  with a fixed  $\beta = N/M$  and  $\mathbf{x} \sim \Phi_S$  (see (4)). In OAMP,  $\mathbf{e}_t^{\eta \rightarrow \hat{\phi}}$  defined in (38a) can be modeled by a sequence of IIDG samples independent of  $\mathbf{x}$ . As shown in Fig. 37(b), the  $\eta_t$  and  $\hat{\phi}_t$  in OAMP can be characterized by the following transfer functions:

$$\rho = \eta_{SE}(v) \equiv v^{-1} - [\hat{\gamma}_{SE}^{-1}(v)]^{-1}, \quad (40a)$$

$$v = \hat{\phi}_{SE}^S(\rho) \equiv \text{mmse}\{\mathbf{x} | \sqrt{\rho} \mathbf{x} + \mathbf{z}, \Phi_S\}, \quad (40b)$$

where  $\mathbf{z} \sim \mathcal{CN}(\mathbf{0}, \mathbf{I})$  is independent of  $\mathbf{x}$ , and  $\hat{\gamma}_{SE}^{-1}(\cdot)$  is the inverse of  $\hat{\gamma}_{SE}(\cdot)$  defined as

$$\hat{\gamma}_{SE}(v) \equiv \text{mmse}\{\mathbf{x} | \mathbf{x} + \sqrt{v} \mathbf{z}, \Gamma\} = \frac{1}{N} \text{tr} \{ [snr \mathbf{A}^H \mathbf{A} + v^{-1} \mathbf{I}]^{-1} \}. \quad (40c)$$

Some instances of  $\hat{\phi}_{SE}^S(\rho)$  for Gaussian signaling and discrete (e.g. QPSK) signaling are provided in Appendix B.

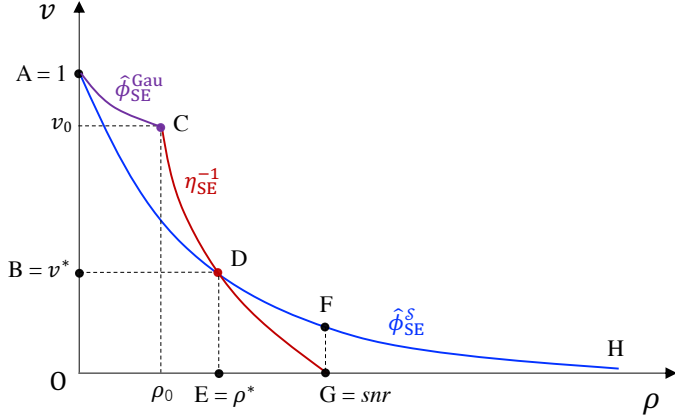


Fig. 5. Graphic illustration of OAMP in the un-coded LUIS. The fixed point  $(\rho^*, v^*)$  gives the MMSE of the LUIS if both  $\eta_t$  and  $\phi_t$  are local MMSE processors.  $\rho_0 = [\gamma_{\text{SE}}(1)]^{-1} - 1$ ,  $v_0 = \gamma_{\text{SE}}^{-1}(\rho_0)$  and  $\eta_{\text{SE}}(0) = \text{snr}$ .

### B. MMSE Achieving Property of OAMP in the Un-Coded LUIS

*Assumption 1:* There is exactly one fixed point for  $\hat{\phi}_{\text{SE}}^S(\rho) = \eta_{\text{SE}}^{-1}(\rho)$  in  $\rho > 0$ , where  $\eta_{\text{SE}}^{-1}(\cdot)$  is the inverse of  $\eta_{\text{SE}}(\cdot)$ .

Fig. 5 provides a graphical illustration of Assumption 1. OAMP converges to a unique fixed point  $(\rho^*, v^*)$  with  $v^* = \hat{\phi}_{\text{SE}}^S(\rho^*)$ . The following lemma is proved in [18], [19].

*Lemma 8 (MMSE Optimal):* Let  $\hat{\mathbf{x}}_{\text{MMSE}} = \mathbb{E}\{\mathbf{x}|\Gamma, \Phi_S\}$  be the conditional mean of  $\mathbf{x}$  given  $\Gamma$  and  $\Phi_S$ . Suppose that Assumption 1 holds. Then

$$v^* \equiv \frac{1}{N} \mathbb{E}\{\|\mathbf{x} - \hat{\mathbf{x}}_{\text{MMSE}}\|^2\}, \quad (41)$$

i.e., OAMP converges to the MMSE of the un-coded LUIS.

### C. Area Properties of LUIS

The following theorem gives the area property of a LUIS.

*Theorem 1 (Area Property of a LUIS):* Suppose that Assumption 1 holds. Then the constrained capacity of a LUIS given  $p_X(x)$  is given by the area  $A_{\text{ADGO}}$  (see Fig. 5) covered by  $\eta_{\text{SE}}^{-1}$  and  $\hat{\phi}_{\text{SE}}^S$ , i.e.,

$$C_{\text{LUIS}}(\text{snr}) = A_{\text{ADGO}}, \quad (42)$$

where

$$A_{\text{ADGO}} = \int_0^{\rho^*} \hat{\phi}_{\text{SE}}^S(\rho) d\rho + \int_{\rho^*}^{\text{snr}} \eta_{\text{SE}}^{-1}(\rho) d\rho \quad (43a)$$

$$= \int_0^{\rho^*} \hat{\phi}_{\text{SE}}^S(\rho) d\rho + \log v^* + \frac{1}{N} \log \det(\mathbf{B}(\rho^*, v^*)), \quad (43b)$$

and  $\mathbf{B}(\rho^*, v^*) = ([v^*]^{-1} - \rho^*)\mathbf{I} + snr\mathbf{A}^H\mathbf{A}$ .

*Proof:* See Appendix C. ■

Based on the above discussions, we can obtain the following interesting area properties as illustrated in Fig. 5.

- Area  $A_{\text{BDEO}}$  is given by

$$A_{\text{BDEO}} = \rho^* v^*, \quad (44)$$

where  $(\rho^*, v^*)$  denotes the unique fixed point C in Fig. 5.

- Area  $A_{\text{AHO}}$  gives the entropy of the constellation, i.e.,

$$A_{\text{AHO}} = \log |\mathcal{S}|, \quad (45)$$

which is the maximum achievable rate in the noiseless case. See Lemma 4.

- Area  $A_{\text{ADGO}}$  gives the constrained capacity  $C_{\text{LUIS}}$  of a LUIS. See Theorem 1.
- Area  $A_{\text{ACGO}}$  gives the Gaussian capacity  $C_{\text{Gau-LUIS}}$  of a LUIS. See Theorem 3. That is,

$$A_{\text{ACGO}} = C_{\text{Gau-LUIS}}(snr) = \frac{1}{N} \log \det (\mathbf{I} + snr\mathbf{A}^H\mathbf{A}). \quad (46)$$

- Area  $A_{\text{ACD}}$  gives the shaping gain of Gaussian signaling. Curve AC denotes the un-coded Gaussian NLE for Gaussian signaling.
- Area  $A_{\text{ADEO}}$  gives the achievable rate of a receiver with an OAMP detector cascaded by a decoder. There is no iteration between the two. That is,

$$A_{\text{ADEO}} = R_{\text{CAS}}(snr) = C_{\text{SISO}}(\rho^*) = \int_0^{\rho^*} \hat{\phi}_{\text{SE}}^{\mathcal{S}}(\rho) d\rho. \quad (47)$$

In this case, OAMP achieves the MMSE by treating the codeword as an IID sequence. However, the overall algorithm is not capacity optimal.

- Area  $A_{\text{DGE}}$  gives the rate loss for the cascading receiver, i.e.,

$$A_{\text{DGE}} = C_{\text{LUIS}}(snr) - R_{\text{CAS}}(snr) = \int_{\rho^*}^{snr} \eta_{\text{SE}}^{-1}(\rho) d\rho = \log v^* + \frac{1}{N} \log \det (\mathbf{B}(\rho^*)). \quad (48)$$

- Area  $A_{\text{AFGO}}$  gives the constrained capacity of a SISO-AWGN channel. See II-C. That is,

$$A_{\text{AFGO}} = C_{\text{SISO}}(snr) = \int_0^{snr} \hat{\phi}_{\text{SE}}^{\mathcal{S}}(\rho) d\rho. \quad (49)$$

- Area  $A_{\text{DFG}}$  gives the capacity gap of a LUIS and parallel SISO channels, i.e.,

$$A_{\text{DFG}} = C_{\text{SISO}}(snr) - C_{\text{LUIS}}(snr) \quad (50a)$$

$$= \int_{\rho^*}^{snr} \hat{\phi}_{\text{SE}}^{\mathcal{S}}(\rho) d\rho - A_{\text{DGE}} \quad (50b)$$

$$= \int_{\rho^*}^{snr} \hat{\phi}_{\text{SE}}^{\mathcal{S}}(\rho) d\rho - \log v^* - \frac{1}{N} \log \det(\mathbf{B}(\rho^*)). \quad (50\text{c})$$

In other words, area  $A_{\text{DFG}}$  gives the rate loss due to the cross-symbol interference in  $\mathbf{A}\mathbf{x}$ . When  $\beta \rightarrow 0$ ,  $\lim_{\beta \rightarrow 0} \mathbf{A}^H \mathbf{A} = \mathbf{I}$ , indicating that the constrained capacity of a LUIS will converge to that of a set of parallel SISO channels in the limiting case. In this case, the cross-symbol interference disappears, so C→E and areas  $A_{\text{DFG}}$  and  $A_{\text{DGE}}$  become negligible. Then, the separate detection and decoding strategy becomes optimal.

- Area  $A_{\text{FHG}}$  gives the rate loss due to the channel noise  $\mathbf{n}$ , i.e.,

$$A_{\text{FHG}} = A_{\text{AHO}} - A_{\text{AFGO}} = \log |\mathcal{S}| - C_{\text{SISO}}(snr) = \int_{snr}^{\infty} \hat{\phi}_{\text{SE}}^{\mathcal{S}}(\rho) d\rho. \quad (51)$$

- Area  $A_{\text{BDGO}}$  is given by

$$A_{\text{BDGO}} = A_{\text{BDEO}} + A_{\text{DGE}} = \rho^* v^* + \log v^* + \frac{1}{N} \log \det(\mathbf{B}(\rho^*)). \quad (52)$$

Following (42), we rewrite the constrained capacity of a LUIS as  $C_{\text{LUIS}} = A_{\text{BDGO}} + A_{\text{ADEO}} - A_{\text{BDEO}}$ . Since  $A_{\text{BDEO}} = \rho^* v^*$  and  $A_{\text{ADEO}} = C_{\text{SISO}}(\rho^*) = I(x; \sqrt{\rho^*}x + z)$ , following (9), we have:

$$\int_0^{snr v^*} \mathcal{R}_{\mathbf{R}}(-z) dz = A_{\text{BDGO}}. \quad (53)$$

## V. ACHIEVABLE RATES OF OAMP IN THE CODED LUIS

For a LUIS involving FEC coding, we rewrite the problem as

$$\text{Linear constraint } \Gamma : \mathbf{y} = \mathbf{A}\mathbf{x} + \mathbf{n}, \quad (54\text{a})$$

$$\text{Code constraint } \Phi_{\mathcal{C}} : \mathbf{x} \in \mathcal{C}, \quad x_i \sim P_X(x), \quad \forall i, \quad (54\text{b})$$

where  $\mathcal{C}$  is a codebook. In this section, we investigate the achievable rate for OAMP with FEC decoding and compare it with the conventional algorithms.

### A. Joint OAMP and APP Decoding

We focus on a joint OAMP and APP decoding scheme for a coded LUIS.

$$\mathbf{x}_t^{\eta \rightarrow \hat{\phi}_{\mathcal{C}}} = \eta_t(\mathbf{x}_t^{\hat{\phi}_{\mathcal{C}} \rightarrow \eta}), \quad (55\text{a})$$

$$\mathbf{x}_{t+1}^{\hat{\phi}_{\mathcal{C}} \rightarrow \eta} = \hat{\phi}_t^{\mathcal{C}}(\mathbf{x}_t^{\eta \rightarrow \hat{\phi}_{\mathcal{C}}}), \quad (55\text{b})$$

where  $\hat{\phi}_t^{\mathcal{C}}$  is an APP decoder for the code constraint  $\mathbf{x} \in \mathcal{C}$ , and  $\eta_t$  is the same as that in (37a). The symbol-wise demodulator  $\hat{\phi}_t^{\mathcal{S}}$  in (37b) for the un-coded LUIS is replaced by an decoder  $\hat{\phi}_t^{\mathcal{C}}$  for a coded LUIS.

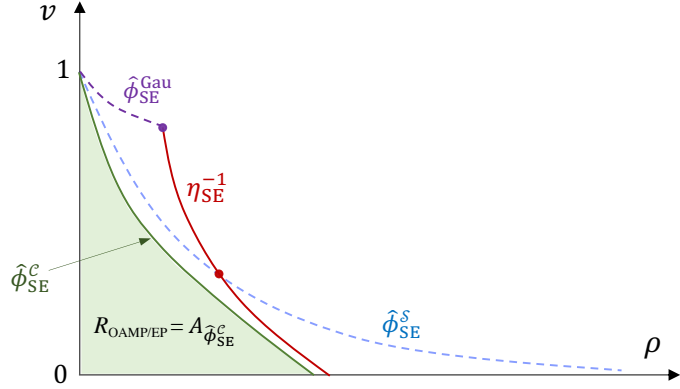


Fig. 6. Graphic illustration of transfer curves:  $\tilde{\eta}^{-1}$ ,  $\tilde{\phi}$  and  $\tilde{\psi}$  in OAMP, where  $\tilde{\phi}$  is a demodulation function (un-coded case) and  $\tilde{\psi}$  is a decoding function (coded case).

Define

$$\mathbf{e}_t^{\hat{\phi}_c \rightarrow \eta} \equiv \mathbf{x}_t^{\hat{\phi}_c \rightarrow \eta} - \mathbf{x}, \quad \rho_t \equiv \frac{1}{N} \mathbb{E} \{ \| \mathbf{e}_t^{\hat{\phi}_c \rightarrow \eta} \|^2 \}, \quad (56a)$$

$$\mathbf{e}_t^{\eta \rightarrow \hat{\phi}_c} \equiv \mathbf{x}_t^{\eta \rightarrow \hat{\phi}_c} - \mathbf{x}, \quad v_t \equiv \frac{1}{N} \mathbb{E} \{ \| \mathbf{e}_t^{\eta \rightarrow \hat{\phi}_c} \|^2 \}. \quad (56b)$$

Lemma 7 gives the IIDG property for OAMP for un-coded  $\mathbf{x}$ . The main discussions of this paper are based on the following assumption for coded  $\mathbf{x}$ .

*Assumption 2 (Asymptotic IIDG):* Let  $M, N \rightarrow \infty$  with a fixed  $\beta = N/M$  and  $\mathbf{x} \sim \Phi_C$  (see (54b)). For OAMP in (55),  $\mathbf{e}_t^{\eta \rightarrow \hat{\phi}_c}$  defined in (56) can be modeled by a sequence of IIDG samples independent of  $\mathbf{x}$ , and  $\eta_t$  and  $\hat{\phi}_t^c$  can be characterized by

$$\rho = \eta_{SE}(v), \quad (57a)$$

$$v = \hat{\phi}_{SE}^c(\rho) \equiv \text{mmse}\{\mathbf{x} | \sqrt{\rho}\mathbf{x} + \mathbf{z}, \Phi_C\}, \quad (57b)$$

where  $\eta_{SE}(\cdot)$  is the same as that in (40).

### B. Curve Matching Principle

In the un-coded case, OAMP converges to a fixed  $(\rho^*, v^*)$  in Fig. 5. Detection is not error-free as  $v^* > 0$ . In the coded case, it is possible to achieve error-free detection using a properly designed  $\hat{\phi}_{SE}^c(\cdot)$ . As illustrated in Fig. 6, the key is to create a detection tunnel that converges to  $v = 0$ , implying zero error rate<sup>4</sup>. There should be no fixed point between  $\hat{\phi}_{SE}^c(\rho)$  and  $\eta_{SE}^{-1}(\rho)$ ,

<sup>4</sup>In fact, we can never do error-free recovery with a finite-length coding. In practice, we can change the error condition to

$$\hat{\phi}_{SE}^c(\rho) < \eta_{SE}^{-1}(\rho), \quad 0 \leq \rho \leq \eta_{SE}(\epsilon),$$

where  $\epsilon$  is the target error of the OAMP receiver. In the simulations of this paper, we set  $\epsilon$  in  $10^{-4} \sim 10^{-5}$ .

since otherwise the tunnel will be closed at  $v > 0$ . This requires

$$\hat{\phi}_{\text{SE}}^{\mathcal{C}}(\rho) < \eta_{\text{SE}}^{-1}(\rho), \quad 0 \leq \rho \leq \text{snr}. \quad (58)$$

Also, the decoder should achieve an MSE lower than that of a symbol-by-symbol detector, i.e.,

$$\hat{\phi}_{\text{SE}}^{\mathcal{C}}(\rho) < \hat{\phi}_{\text{SE}}^{\mathcal{S}}(\rho), \quad \text{for } \rho \geq 0. \quad (59)$$

Combining (58) and (59), we obtain a necessary and sufficient condition for OAMP to achieve error-free detection:

$$\hat{\phi}_{\text{SE}}^{\mathcal{C}}(\rho) < \hat{\phi}_{\text{SE}}^*(\rho) \equiv \min\{\eta_{\text{SE}}^{-1}(\rho), \hat{\phi}_{\text{SE}}^{\mathcal{S}}(\rho)\}, \quad 0 \leq \rho < \text{snr}. \quad (60)$$

### C. Achievable Rate and Capacity Optimality of OAMP

Following Lemma 4 and the error-free condition in (60), the achievable rate of OAMP receiver is given by

$$R_{\text{OAMP}}(\text{snr}) = \int_0^{\infty} \hat{\phi}_{\text{SE}}^{\mathcal{C}}(\rho) d\rho, \quad \hat{\phi}_{\text{SE}}^{\mathcal{C}}(\rho) < \hat{\phi}_{\text{SE}}^*(\rho). \quad (61)$$

That is, error-free detection can be achieved by the OAMP receiver if  $R_{\mathcal{C}} \leq R_{\text{OAMP}}$ .

*Theorem 2 (Capacity Optimality):* Suppose that Assumption 1 and Assumption 2 hold. Then, the achievable rate of OAMP achieves the constrained capacity, i.e.,

$$R_{\text{OAMP}}(\text{snr}) \rightarrow C_{\text{LUIS}}(\text{snr}), \quad (62)$$

if  $\hat{\phi}_{\text{SE}}^{\mathcal{C}}(\rho) \rightarrow \hat{\phi}_{\text{SE}}^*(\rho)$  in  $[0, \text{snr}]$ .

Some notes of Theorem 2 are in order.

- Theorem 2 is based on a matching condition:

$$\hat{\phi}_{\text{SE}}^{\mathcal{C}}(\rho) \rightarrow \hat{\phi}_{\text{SE}}^*(\rho). \quad (63)$$

An existence proof of a code achieving (63) can be found in Appendix C-B [20] for Gaussian signaling. For other signaling, the code existence is a conjecture only. Some numerical results will be provided in VI to approximately achieve (63) for QPSK modulations.

- The situations for multi-ary modulations are more complicated. Various techniques have been developed to match the extrinsic information transfer (EXIT) functions of local processors in Turbo receivers [46]–[48]. These methods can be used to achieve (63) approximately. Detailed discussions on the multi-ary systems are beyond the scope of this paper.
- Interestingly, the discussions above provide an alternative proof for the constrained capacity of a LUIS. The key is to prove  $A_{\text{ADGO}} = C_{\text{LUIS}}(\text{snr})$  without prompting the result in [18]. This is indeed possible using the properties of OAMP directly. The details can be found in Appendix D.

#### D. Gaussian Signaling Case

We now study a special case of V-C when  $\mathbf{x}$  is Gaussian. For general signaling, Assumption 1 does not always hold. However, in Gaussian signaling, we show that Assumption 1 asymptotically holds. In addition, the constrained capacity are reduced to the well-known Gaussian capacity.

*Lemma 9 (Unique Fixed Point):* For a LUIS with Gaussian signaling  $\mathbf{x} \sim \mathcal{CN}(\mathbf{0}, \mathbf{I})$ , Assumption 1 asymptotically holds. That is, equation  $\hat{\phi}_{\text{SE}}^{\mathcal{S}}(\rho) = \eta_{\text{SE}}^{-1}(\rho)$  has a unique positive solution:

$$\rho_{\text{Gau}}^* = [\hat{\gamma}_{\text{SE}}(1)]^{-1} - 1. \quad (64)$$

*Proof:* For Gaussian signaling, we have [49]

$$\hat{\phi}_{\text{SE}}^{\mathcal{S}}(\rho) = \hat{\phi}_{\text{SE}}^{\text{Gau}}(\rho) = 1/(1 + \rho). \quad (65)$$

Substituting (40a) and (65) into  $\hat{\phi}_{\text{SE}}^{\text{Gau}}(\rho) = \eta_{\text{SE}}^{-1}(\rho)$ , we obtain (64). Since  $\hat{\gamma}_{\text{SE}}(1) = \text{mmse}\{\mathbf{x}|\mathbf{x} + \mathbf{z}, \Gamma\}$  is monotonous and less than 1,  $\rho_{\text{Gau}}^*$  is positive and unique. ■

*Lemma 10 (Existence of Curve-Matched Code):* For Gaussian signaling, there exists an  $n$ -layer superposition coded modulation (SCM) code with transfer function  $\hat{\phi}_{\text{SE}}^{\mathcal{C}}(\rho) \rightarrow \hat{\phi}_{\text{SE}}^*(\rho)$  in  $[0, \text{snr}]$  as  $n \rightarrow \infty$ .

*Proof:* The proof is omitted as it is the same as that in Appendix C-B [20]. ■

Based on Lemma 9 and Lemma 10, we have the following theorem for Gaussian signaling.

*Theorem 3:* The Gaussian capacity of a LUIS is given by  $A_{\text{ACGO}}$ , i.e.,

$$C_{\text{Gau-LUIS}}(\text{snr}) = A_{\text{ACGO}}, \quad (66)$$

where

$$A_{\text{ACGO}} = \frac{1}{N} \log \det (\mathbf{I} + \text{snr} \mathbf{A}^H \mathbf{A}). \quad (67)$$

Furthermore, suppose that Assumption 2 holds. Then, the achievable rate of OAMP achieves the Gaussian capacity, i.e.,

$$R_{\text{OAMP}}(\text{snr}) \rightarrow C_{\text{Gau-LUIS}}(\text{snr}). \quad (68)$$

*Proof:* For Gaussian signaling, we have  $\hat{\phi}_{\text{SE}}^{\mathcal{S}}(\rho) = \hat{\phi}_{\text{SE}}^{\text{Gau}}(\rho) = 1/(1 + \rho)$ , we have

$$\int_0^{\rho^*} \hat{\phi}_{\text{SE}}^{\mathcal{S}}(\rho) d\rho + \log \hat{\phi}_{\text{SE}}^{\mathcal{S}}(\rho^*) = 0. \quad (69)$$

Then, following Theorem 2, we have

$$R_{\text{OAMP}}(\text{snr}) = A_{\text{ADGO}} \quad (70a)$$

$$= \frac{1}{N} \log \det (\mathbf{B}(1)) \quad (70b)$$

$$= \frac{1}{N} \log \det (\mathbf{I} + \text{snr} \mathbf{A}^H \mathbf{A}), \quad (70c)$$

which is the same as the Gaussian capacity given in (8). Thus, we have

$$C_{\text{Gau-LUIS}}(snr) = A_{\text{ACGO}}. \quad (71)$$

Thus, we obtain Theorem 3.  $\blacksquare$

### E. Comparisons with Alternative Algorithms

1) *Comparing with Conventional Turbo*: Turbo is extrinsic that requires independent input-output errors of each local processor. OAMP only requires orthogonal input-output errors, which is generally less stringent than the independent requirement. It was proved in [32] that the MSE of OAMP is lower than Turbo (whose achievable rate was given in [13]). That is,  $\eta_{\text{SE-OAMP}}^{-1} \geq \eta_{\text{SE-Turbo}}^{-1}$ . As a result, the achievable rate of OAMP is not less than Turbo.

Fig. 7 shows the achievable rates of Turbo [13] and OAMP. Both Turbo and OAMP achieve the Gaussian capacity. However, for QPSK, 8PSK and 16QAM modulations, OAMP achieves the constrained capacity when the corresponding OAMP has a unique fixed point, while Turbo always has rate loss. Similar results can be obtained for other non-Gaussian signaling. Therefore, OAMP outperforms Turbo, which is consistent with the result in [32]. In addition, the gap between OAMP and Turbo increases with  $\beta$  and  $\kappa$  (condition number), and the gap is negligible if  $\beta$  and  $\kappa$  are small.

2) *Comparison with Cascading OAMP and Decoding*: We define a cascading OAMP and decoding (CAS-OAMP) scheme [49], [50] as following. We run OAMP until it converges. The result is used by decoder. There is no iteration between OAMP and the decoder. Area  $A_{\text{ADEO}}$  in Fig. 5 denotes the achievable rate of CAS-OAMP

$$A_{\text{ADEO}} = R_{\text{CAS}}(snr) = \int_0^{\rho^*} \hat{\phi}_{\text{SE}}^{\mathcal{S}}(\rho) d\rho. \quad (72)$$

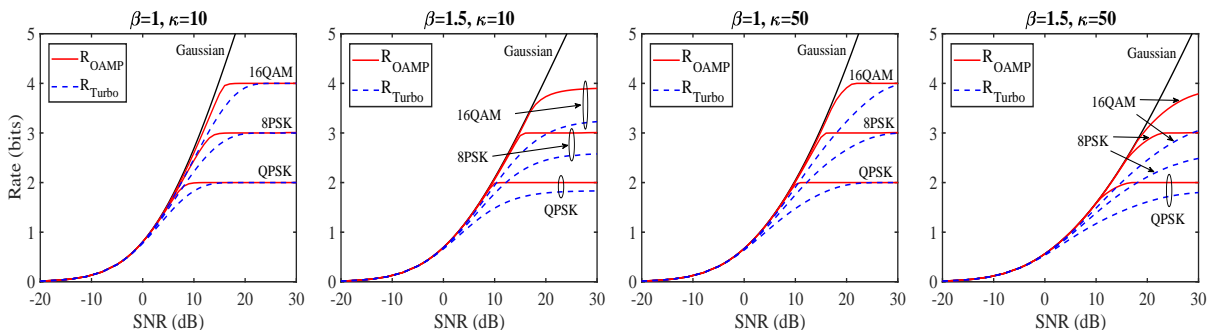


Fig. 7. Comparison between the achievable rates of Turbo and OAMP of linear systems with  $\beta = N/M = \{1, 1.5\}$  and  $\kappa = \{10, 50\}$  (condition numbers). QPSK, 8PSK, 16QAM and Gaussian modulations are considered.

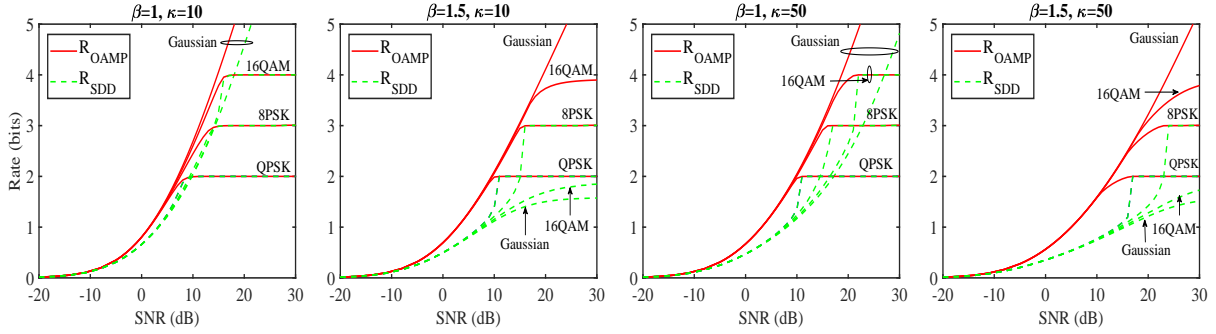


Fig. 8. Comparison between the achievable rates of CAS-OAMP and OAMP of linear systems with  $\beta = N/M = \{1, 1.5\}$  and  $\kappa = \{10, 50\}$  (condition numbers). QPSK, 8PSK, 16QAM and Gaussian modulations are considered.

Comparing (72) with the  $R_{\text{OAMP}}$  in Theorem 2 (see (42) and (62)), the rate loss of CAS-OAMP is given by the area  $A_{\text{DGE}}$  in Fig. 5:

$$\Delta R_{\text{CAS}} = A_{\text{DGE}} = \log v^* + \frac{1}{N} \log \det(\mathbf{B}(\rho^*)). \quad (73)$$

For Gaussian signaling,

$$R_{\text{CAS}} = \log(1 + \rho_{\text{Gau}}^*). \quad (74)$$

Fig. 8 shows the achievable rates of CAS-OAMP [49], [50] and OAMP. As it can be seen, OAMP outperforms CAS-OAMP, and their gap increases with  $\beta$  and  $\kappa$  (condition number). Note that there are rate jumps in CAS-OAMP due to the discontinuity of the first fixed point of OAMP. Please refer to [20] for more details.

## VI. NUMERIC RESULTS

This section discusses matching techniques using optimized irregular LDPC codes and QPSK modulation. Simulation results will be provided. We will not go to the detailed code design process as it is the same as that in Section IV-A of [20]. For higher order modulation, the design of a curve-matching code becomes more complicated. We leave the code design for high-order modulations as our future work.

*Ill-Conditioned Matrix Generation:* Let the SVD of  $\mathbf{A}$  be  $\mathbf{A} = \mathbf{U}\Sigma\mathbf{V}$ . In all the simulations, we set the eigenvalues  $\{d_i\}$  in  $\Sigma$  as [51]:  $d_i/d_{i+1} = \kappa^{1/T}$  for  $i = 1, \dots, T-1$  and  $\sum_{i=1}^T d_i^2 = N$ , where  $T = \min\{M, N\}$ . Here,  $\kappa \geq 1$  controls the condition number of  $\mathbf{A}$ .

### A. Irregular LDPC Code Optimization for OAMP

Fig. 9 provides the BER simulations for the LUIS, in which  $\mathbf{x}$  is generated using optimized irregular LDPC codes [52], [53] with codeword length =  $10^5$ . The receiver denoted as ‘‘OAMP-Irrg’’ consists of two parts as shown in Fig. 3. The NLD in Fig. 3 is implemented

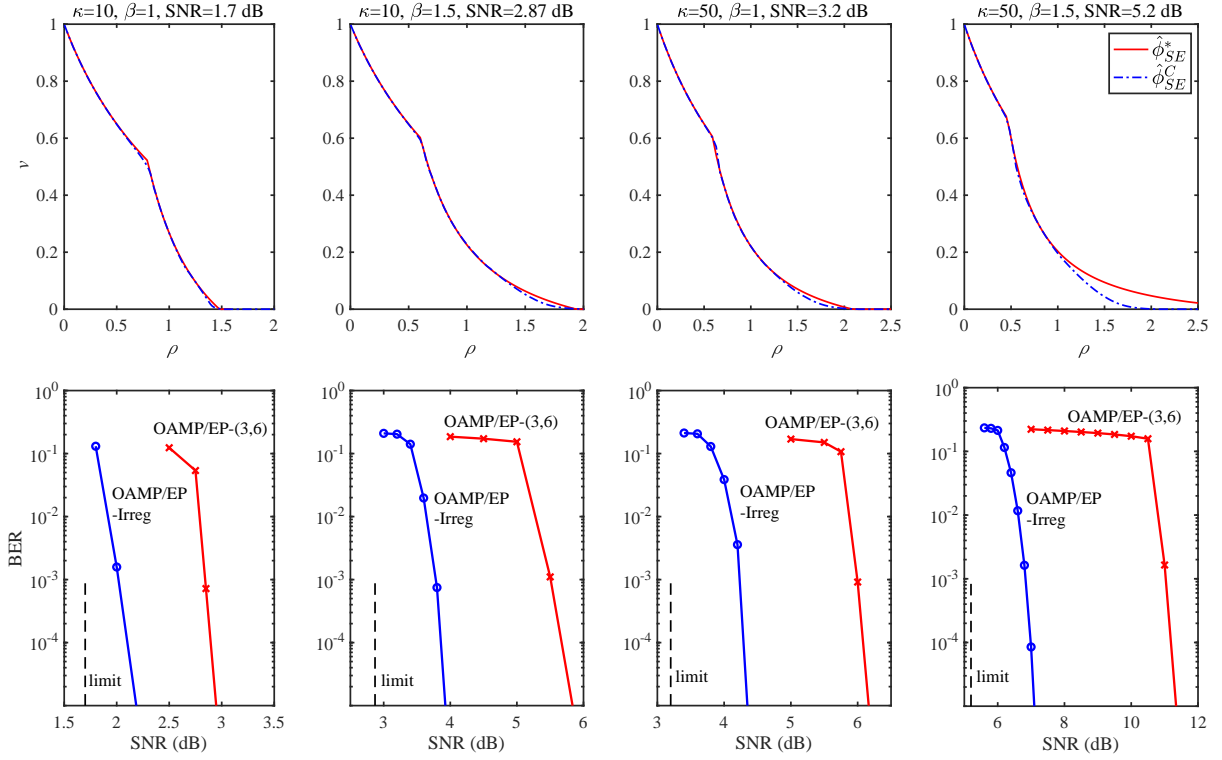


Fig. 9. Transfer curve matching and BER performances of OAMP, where “ $\hat{\phi}_{SE}^*$ ” denotes the fully matched transfer curve of OAMP (target), “ $\hat{\phi}_{SE}^C$ ” the optimized NLD of OAMP, “OAMP-Irreg” the BER of optimized irregular LDPC codes, “OAMP-(3, 6)” the BER with regular (3, 6) LDPC codes. Codeword length =  $10^5$ , code rate  $\approx 0.5$ , QPSK modulation, and iterations = 250, and  $\beta = N/M = \{1, 1.5\}$ . For more details, refer to Table I.

using a standard sum-product decoder. The channel loads are  $\beta = \{1, 1.5\}$  with  $(N, M) = (500, 500)$  and  $(500, 333)$ , respectively. The ill-conditional numbers are  $\kappa = \{10, 50\}$ . The corresponding optimized code parameters are given in Table I, which illustrate that these decoding thresholds are very close (about  $0.1 \text{ dB} \sim 0.2 \text{ dB}$  away) to the Shannon limits.

To verify the finite-length performance of the irregular LDPC codes with code rate  $\approx 0.5$ , we provide the BER performances of the optimized codes. QPSK modulation is used, the rate of each symbol is  $R \approx 1$  bits/symbol, and the sum rate is  $R_{\text{sum}} \approx N$  bits per channel use. The maximum iteration number is 250. Fig. 9 shows that for all  $\beta$  and  $\kappa$ , gaps between the BER curves of the codes at  $10^{-5}$  and the corresponding Shannon limits are about 1 dB.

*Comparison with Un-Optimized Regular LDPC Code:* To validate the advantage of the proposed system through matching between LD and optimized irregular codes, we provide the state-of-art system for comparison, which are OAMP detection combined with the standard regular (3, 6) LDPC code (denoted as “(3, 6)”) [10], corresponding to  $R_{\text{CAS}}$  discussed in Section V-E. As shown in Fig. 9, when the BER curves of two systems are at  $10^{-5}$ , the optimized irregular LDPC codes have  $0.8 \sim 4$  dB performance gains over the un-optimized regular (3, 6) LDPC code for  $\beta = \{1, 1.5\}$  and  $\kappa = \{10, 50\}$ . These demonstrate that code optimization provides a promising performance improvement for OAMP, especially for the large  $\beta$  and  $\kappa$ .

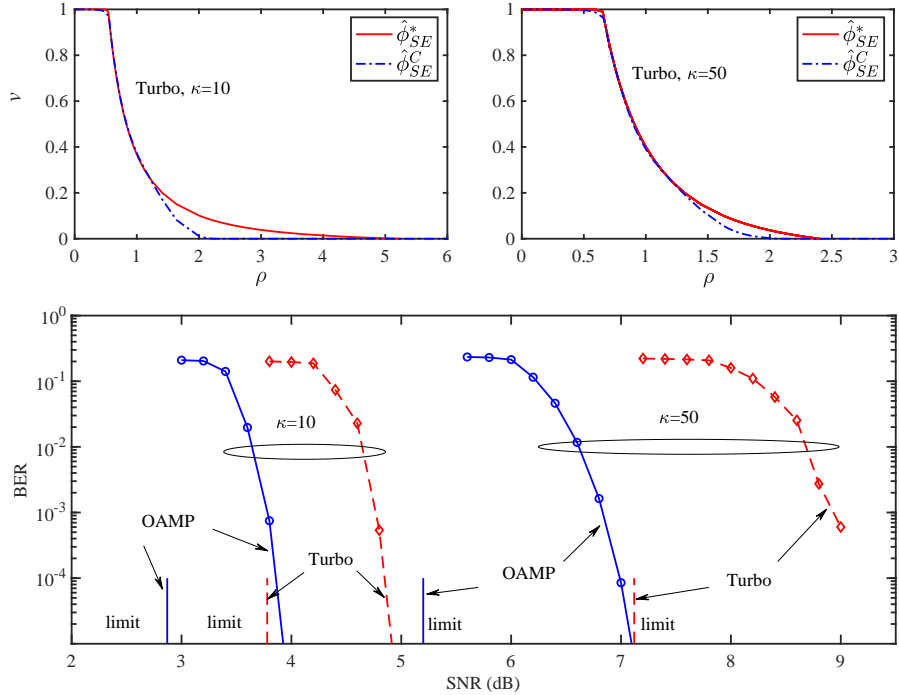


Fig. 10. Transfer curve matching of Turbo, and BER performances of OAMP and Turbo [14], [15] with optimized irregular LDPC codes, where “ $\hat{\phi}_{SE}^*$ ” and “ $\hat{\phi}_{SE}^C$ ” denotes the target and the optimized transfer curves of Turbo, “limit” the QPSK rate limits of OAMP or Turbo. Codeword length =  $10^5$ , code rate  $\approx 0.5$ , QPSK modulation, and iterations = 250, and  $\beta = 2$  with  $N = 500$  and  $M = 333$ . For more details, refer to Table I.

### B. Comparison of OAMP and Turbo

To compare OAMP with the conventional Turbo [14], [15], we consider a  $500 \times 333$  QPSK linear system with  $\beta = 1.5$  and  $\kappa = \{10, 50\}$ . As shown in Fig. 7, the SNR limits of OAMP and Turbo for the target rate  $R = 1$  are respectively 2.85 dB and 3.78 dB for  $\kappa = 10$ , and 5.03 dB and 7.12 dB for  $\kappa = 50$ . The upper two sub-figures in Fig. 10 shows the transfer curve matching of Turbo, where the irregular LDPC codes (code length =  $10^5$  code rate = 0.5) are respectively optimized respectively Turbo. The curve matching of OAMP can be found in Fig. 9. Note that the NLD of OAMP denotes the *a-posteriori* output variance, while the NLD of Turbo denotes the *extrinsic* output variance. The third sub-figure in Fig. 10 shows the BER performances of the optimized OAMP and the optimized Turbo (with iterations = 250). The corresponding optimized code parameters are given in Table I, which illustrate that these decoding thresholds are very close (about 0.1 dB~0.2 dB away) to the capacity limits. In addition, their simulated BERs of OAMP and Turbo are about 1dB for  $\kappa = 10$  and 2 dB for  $\kappa = 50$  away from their thresholds respectively. For more details, please refer to Table I. As a result, comparing with the Turbo, OAMP has 1 dB improvement for  $\kappa = 10$  and 2 dB improvement for  $\kappa = 50$  in BER performance. Overall, the conventional Turbo has huge performance loss in general discrete linear systems, especially in the case of high transmission rate and high ill-conditional number,

TABLE I  
OPTIMIZED IRREGULAR LDPC CODES FOR OAMP AND TURBO

Methods	OAMP				Turbo	
	10	50	10	50		
$\kappa$	1	1.5	1		1.5	
$\beta$				500		
$N$						
$M$	500	333	500		333	
Codeword length				$10^5$		
Target code rate				0.5		
Designed code rate	0.5087	0.5062	0.5075	0.4721	0.5008	0.48635
$R_C$	1.0178	1.0124	1.0150	0.9442	1.0016	0.9727
$R_{\text{sum}}$	508.9	506.2	507.5	472.1	500.8	486.4
Iterations				250		
Check edge distribution	$\eta_7 = 1$	$\eta_8 = 1$	$\eta_8 = 1$	$\eta_7 = 1$	$\eta_8 = 1$	$\eta_6 = 0.2$ $\eta_{12} = 0.8$
Variable edge distribution	$\lambda_2 = 0.3707$ $\lambda_3 = 0.2329$ $\lambda_9 = 0.1815$ $\lambda_{10} = 0.0002$ $\lambda_{27} = 0.0003$ $\lambda_{28} = 0.1516$ $\lambda_{29} = 0.0620$ $\lambda_{30} = 0.0005$	$\lambda_2 = 0.4233$ $\lambda_3 = 0.0677$ $\lambda_{15} = 0.0053$ $\lambda_{16} = 0.2586$ $\lambda_{80} = 0.1426$ $\lambda_{200} = 0.1025$	$\lambda_2 = 0.4624$ $\lambda_3 = 0.0028$ $\lambda_{14} = 0.1924$ $\lambda_{15} = 0.0743$ $\lambda_{70} = 0.1649$ $\lambda_{150} = 0.0322$ $\lambda_{200} = 0.0711$	$\lambda_2 = 0.5082$ $\lambda_{21} = 0.3238$ $\lambda_{22} = 0.0002$ $\lambda_{130} = 0.0001$ $\lambda_{140} = 0.0005$ $\lambda_{150} = 0.0018$ $\lambda_{200} = 0.1652$	$\lambda_2 = 0.4400$ $\lambda_{10} = 0.0577$ $\lambda_{11} = 0.2256$ $\lambda_{50} = 0.0401$ $\lambda_{60} = 0.1665$ $\lambda_{250} = 0.0298$ $\lambda_{300} = 0.0403$	$\lambda_2 = 0.3377$ $\lambda_{12} = 0.0481$ $\lambda_{13} = 0.2288$ $\lambda_{60} = 0.1012$ $\lambda_{70} = 0.1454$ $\lambda_{300} = 0.1388$
(SNR) <sup>*</sup> <sub>dB</sub>	1.7	2.87	3.2	5.2	3.8	7.2
Capacity	1.55	2.85	3.15	5.03	3.78	7.12

while OAMP can approach the discrete system capacity with proper code design (see Fig. 9 also for more simulation results).

*Complexity:* OAMP and Turbo have the same complexity, i.e.,

$$\mathcal{O}((\Xi_{LD} + \Xi_{NLD})N_{ite}), \quad (75)$$

where  $N_{ite}$  is the number of iterations,  $\Xi_{LD}$  and  $\Xi_{NLD}$  the complexities of LD and NLD per iteration respectively. For LDPC coded NLD,  $\Xi_{NLD} \approx 4\bar{d}_v N_C$ , where  $N_C$  is the code length,  $\bar{d}_v = \left( \sum_i \lambda_i / i \right)$  the averaged variable-node degree, and  $\{\lambda_i\}$  the variable-node degree distribution. The complexity of LD is  $\Xi_{LD} = \mathcal{O}(MN^2)$  due to the matrix inverse in LMMSE.

## VII. CONCLUSION

This paper considers an OAMP receiver for a coded LUIS with a unitarily invariant sensing matrix and an arbitrary input distribution. A universal Gram-Schmidt orthogonalization is developed for orthogonal approximate message passing (OAMP). Numerous area properties are established using the established properties of OAMP. We show that OAMP is information theoretically optimal using a curve matching principle and the IIDG assumption. In addition, a coding principle is provided for OAMP, and the irregular LDPC codes are considered for binary signaling as an example. The numerical results show that OAMP is capacity-approaching based on optimized irregular LDPC codes, and significant performance improvements (0.75 dB  $\sim$  4 dB)

are observed over the system without code optimization. Apart from that, OAMP significantly outperforms the well-known Turbo-LMMSE algorithm.

The proof of Assumption 2 is an interesting future work. A rigorous SE proof for a certain kind of non-separable (e.g. uniformly Lipschitz) functions was established in [56] for AMP, which may be used to prove Assumption 2 in this paper.

## APPENDIX A PROOF OF PROPOSITION 1

Let  $\hat{\mathbf{f}} \equiv \hat{f}(\mathbf{x}_{\text{in}})$ . From the orthogonal principle [54] of MMSE estimation,

$$\mathbb{E}\{\mathbf{x}_{\text{in}}^H(\hat{\mathbf{f}} - \mathbf{x})\} = 0, \quad (76a)$$

$$\mathbb{E}\{\hat{\mathbf{f}}^H(\hat{\mathbf{f}} - \mathbf{x})\} = 0. \quad (76b)$$

Assume  $\hat{\mathbf{f}} = \alpha_{\hat{f}} \mathbf{x} + \boldsymbol{\xi}_{\hat{f}}$  with  $\mathbb{E}\{\mathbf{x}^H \boldsymbol{\xi}_{\hat{f}}\} = 0$ . We further have

$$\mathbb{E}\{\boldsymbol{\xi}_{\text{in}}^H \hat{\mathbf{f}}\} = \mathbb{E}\{\boldsymbol{\xi}_{\text{in}}^H \boldsymbol{\xi}_{\hat{f}}\} = (1 - \alpha_{\hat{f}})\mathbb{E}\{\|\mathbf{x}\|^2\}, \quad (77a)$$

$$\mathbb{E}\{\|\hat{\mathbf{f}} - \mathbf{x}\|^2\} = \mathbb{E}\{-\mathbf{x}^H(\hat{\mathbf{f}} - \mathbf{x})\} = (1 - \alpha_{\hat{f}})\mathbb{E}\{\|\mathbf{x}\|^2\}. \quad (77b)$$

where (77a) follows (76a) and  $\mathbb{E}\{\boldsymbol{\xi}_{\text{in}}^H \mathbf{x}\} = 0$ , and (77b) follows (76b) and  $\mathbb{E}\{\boldsymbol{\xi}_{\hat{f}}^H \mathbf{x}\} = 0$ . From (77), we have

$$\frac{1}{N}\mathbb{E}\{\boldsymbol{\xi}_{\text{in}}^H \hat{\mathbf{f}}\} = \frac{1}{N}\mathbb{E}\{\|\hat{\mathbf{f}} - \mathbf{x}\|^2\} = v_{\hat{f}}. \quad (78)$$

From (78) and (23), we obtain (30).

## APPENDIX B INSTANCES OF MMSE TRANSFER FUNCTION $\hat{\phi}_{\text{SE}}^{\mathcal{S}}(\cdot)$

For Gaussian signaling  $x \sim \mathcal{CN}(0, 1)$ ,

$$\hat{\phi}_{\text{SE}}^{\mathcal{S}}(\rho) = \hat{\phi}_{\text{SE}}^{\text{Gau}}(\rho) \equiv 1/(1 + \rho). \quad (79a)$$

For any discrete constellation  $\mathcal{S} = \{s_1, \dots, s_{|\mathcal{S}|}\}$  with probability  $\{q_l\}_{l=1}^{|\mathcal{S}|}$  [55],

$$\hat{\phi}_{\text{SE}}^{\mathcal{S}}(\rho) = 1 - \frac{1}{\pi} \int \frac{\left| \sum_{l=1}^{|\mathcal{S}|} q_l s_l e^{-|y - \sqrt{\rho} s_l|^2} \right|^2}{\sum_{l=1}^{|\mathcal{S}|} q_l e^{-|y - \sqrt{\rho} s_l|^2}} dy, \quad (79b)$$

where the integral is over the complex field. For example, for quadrature phase-shift keying (QPSK) signaling  $x \sim \{\frac{1}{\sqrt{2}}(\pm 1 \pm j)\}$  [37], it can be simplified to

$$\hat{\phi}_{\text{SE}}^{\mathcal{S}}(\rho) = \tilde{\phi}_{\text{SE}}^{\text{QPSK}}(\rho) \equiv 1 - \int_{-\infty}^{\infty} \frac{e^{-y^2/2}}{\sqrt{2\pi}} \tanh(\rho - \sqrt{\rho}y) dy. \quad (79c)$$

## APPENDIX C

### PROOF OF THEOREM 1

In order to prove Theorem 1, we first prove the area expression in (43), and then prove the area property  $A_{\text{ADGO}} = C_{\text{LUIS}}(\text{snr})$ .

#### A. Proof of area expression in (43)

Eqn. (43a) is straightforward. We next prove (43b). For simplicity, we define  $\mathbf{D}(s) = s\mathbf{I} + \text{snr}\mathbf{A}^H\mathbf{A}$ . Then

$$\int_{\rho^*}^{\text{snr}} \eta_{\text{SE}}^{-1}(\rho) d\rho \quad (80\text{a})$$

$$= \int_{v=v^*}^{v=0} v d \left( v^{-1} - [\hat{\gamma}_{\text{SE}}^{-1}(v)]^{-1} \right) \quad (80\text{b})$$

$$= [-\log v]_{v=v^*}^{v=0} - \int_{v=v^*}^{v=0} v d [\hat{\gamma}_{\text{SE}}^{-1}(v)]^{-1} \quad (80\text{c})$$

$$= [-\log v]_{v=v^*}^{v=0} - \int_{[v^*]^{-1}-\rho^*}^{\infty} \hat{\gamma}_{\text{SE}}(s^{-1}) ds \quad (80\text{d})$$

$$= [-\log v]_{v=v^*}^{v=0} - \int_{[v^*]^{-1}-\rho^*}^{\infty} \frac{1}{N} \text{tr}\{[\mathbf{D}(s)]^{-1}\} ds \quad (80\text{e})$$

$$= [-\log v]_{v=v^*}^{v=0} - [\frac{1}{N} \log \det(\mathbf{D}(s))]_{s=[v^*]^{-1}-\rho^*}^{s=\infty} \quad (80\text{f})$$

$$= \log v^* + \frac{1}{N} \log \det(\mathbf{B}(\rho^*, v^*)), \quad (80\text{g})$$

where (80b) follows  $\eta_{\text{SE}}(\rho) = v^{-1} - [\hat{\gamma}_{\text{SE}}^{-1}(v)]^{-1}$ , (80d) follows  $s = [\hat{\gamma}_{\text{SE}}^{-1}(v)]^{-1}$ ,  $\hat{\gamma}_{\text{SE}}^{-1}(0) = 0$  and the fix-point equation  $[\hat{\gamma}_{\text{SE}}^{-1}(v^*)]^{-1} = [v^*]^{-1} - \rho^*$ , (80e) follows  $\int \text{tr}\{(s\mathbf{I} + \mathbf{A})^{-1}\} ds = \log \det(s\mathbf{I} + \mathbf{A})$ , and (80g) follows  $-\lim_{v \rightarrow 0} \log v - \lim_{s \rightarrow \infty} \frac{1}{N} \log \det(\mathbf{D}(s)) = 0$ . Therefore, we obtain the desired (43b) from (43a) and (80).

#### B. Proof of the Area Property $A_{\text{ADGO}} = C_{\text{LUIS}}(\text{snr})$

We now show  $A_{\text{ADGO}} = C_{\text{LUIS}}(\text{snr})$ , where  $A_{\text{ADGO}}$  is given in (43) and  $C_{\text{LUIS}}(\text{snr})$  in (9) that is derived in [18]. First, we will show the consistency of the fixed points in (43) and (9). Then, we show the consistency of  $C_{\text{LUIS}}(\text{snr})$  and  $A_{\text{ADGO}}$ .

1) *Consistency of the Fixed Points:* The following proof is based on an identity

$$\mathcal{R}_{\mathbf{R}}(z) = \mathcal{S}_{\mathbf{R}}^{-1}(-z) - z^{-1}, \quad (81)$$

where  $\mathcal{S}_{\mathbf{R}}^{-1}(\cdot)$  is the inverse of the *Stieltjes transform*  $\mathcal{S}_{\mathbf{R}}(z) = \text{E}_{\lambda_{\mathbf{R}}}\{1/(\lambda_{\mathbf{R}} - z)\}$ . Recall that  $\rho^*$  in (43) is the solution of

$$\eta_{\text{SE}}^{-1}(\rho) = \hat{\phi}_{\text{SE}}^{\mathcal{S}}(\rho), \quad (82\text{a})$$

where  $\eta_{\text{SE}}^{-1}(\cdot)$  is the inverse of

$$\eta_{\text{SE}}(v) \equiv v^{-1} - [\hat{\gamma}_{\text{SE}}^{-1}(v)]^{-1}, \quad (82\text{b})$$

and  $\hat{\gamma}_{\text{SE}}^{-1}(\cdot)$  is the inverse of

$$\hat{\gamma}_{\text{SE}}(v) = \frac{1}{N} \text{tr} \{ [snr \mathbf{A}^H \mathbf{A} + v^{-1} \mathbf{I}]^{-1} \} = snr^{-1} \mathcal{S}_{\mathbf{R}}(- (snr v)^{-1}). \quad (82\text{c})$$

Eqn. (82) can be rewritten to

$$\hat{\phi}_{\text{SE}}^{\mathcal{S}}(\rho) = \hat{\gamma}_{\text{SE}} \left( ([\hat{\phi}_{\text{SE}}^{\mathcal{S}}(\rho)]^{-1} - \rho)^{-1} \right). \quad (83)$$

Substituting (82c) into (83), we have

$$snr \hat{\phi}_{\text{SE}}^{\mathcal{S}}(\rho) = \mathcal{S}_{\mathbf{R}} \left( - snr^{-1} ([\hat{\phi}_{\text{SE}}^{\mathcal{S}}(\rho)]^{-1} - \rho) \right). \quad (84)$$

Taking the inverse  $\mathcal{S}_{\mathbf{R}}^{-1}$  at both sides of (84), we have

$$\mathcal{S}_{\mathbf{R}}^{-1} (snr \hat{\phi}_{\text{SE}}^{\mathcal{S}}(\rho)) = -snr^{-1} ([\hat{\phi}_{\text{SE}}^{\mathcal{S}}(\rho)]^{-1} - \rho). \quad (85)$$

Using (81), we obtain

$$\rho = snr \mathcal{R}_{\mathbf{R}}(-snr \hat{\phi}_{\text{SE}}^{\mathcal{S}}(\rho)), \quad (86)$$

which is the same as the fixed point equation in (43). Therefore,  $\rho^*$  in Lemma 2 and (43) are the same.

2) *Consistency of  $C_{\text{LUIS}}(snr)$  and  $A_{\text{ADGO}}$* : Recall (43):

$$A_{\text{ADGO}} = \int_0^{\rho^*} \hat{\phi}_{\text{SE}}^{\mathcal{S}}(\rho) d\rho + \int_{\rho^*}^{snr} \eta_{\text{SE}}^{-1}(\rho) d\rho \quad (87)$$

Based on the *I-MMSE Lemma*, we have

$$\int_0^{\rho^*} \hat{\phi}_{\text{SE}}^{\mathcal{S}}(\rho) d\rho = I(x; \sqrt{\rho^*} x + z). \quad (88)$$

Furthermore,

$$\int_{\rho^*}^{snr} \eta_{\text{SE}}^{-1}(\rho) d\rho \quad (89\text{a})$$

$$= \int_{v=v^*}^{v=0} v d \left( v^{-1} - [\hat{\gamma}_{\text{SE}}^{-1}(v)]^{-1} \right) \quad (89\text{b})$$

$$= \int_{s=[v^*]^{-1}-\rho^*}^{s=\infty} \hat{\gamma}_{\text{SE}}(s^{-1}) d \left( [\hat{\gamma}_{\text{SE}}(s^{-1})]^{-1} - s \right) \quad (89\text{c})$$

$$= \int_{s=[v^*]^{-1}-\rho^*}^{s=\infty} \mathcal{S}_{\mathbf{R}}(-snr^{-1}s) d \left( [\mathcal{S}_{\mathbf{R}}(-snr^{-1}s)]^{-1} - snr^{-1}s \right) \quad (89\text{d})$$

$$= - \int_{t=-\infty}^{t=-snr^{-1}([v^*]^{-1}-\rho^*)} \mathcal{S}_R(t) d(\mathcal{S}_R(t)^{-1} + t) \quad (89e)$$

$$= - \int_0^{snr v^*} z d\mathcal{R}_R(-z) \quad (89f)$$

$$= \int_0^{snr v^*} \mathcal{R}_R(-z) dz + [z\mathcal{R}_R(-z)]_{z=snr v^*}^{z=0} \quad (89g)$$

$$= \int_0^{snr v^*} \mathcal{R}_R(-z) dz - \rho^* v^*, \quad (89h)$$

where (89b) follows  $\eta_{\text{SE}}(\rho) = v^{-1} - [\hat{\gamma}_{\text{SE}}^{-1}(v)]^{-1}$ , (89c) follows  $s = [\hat{\gamma}_{\text{SE}}^{-1}(v)]^{-1}$ ,  $\hat{\gamma}_{\text{SE}}^{-1}(0) = 0$  and the fix-point equation  $[\hat{\gamma}_{\text{SE}}^{-1}(v^*)]^{-1} = [v^*]^{-1} - \rho^*$ , (89d) follows  $\hat{\gamma}_{\text{SE}}(v) = snr^{-1} \mathcal{S}_R(-(snr v)^{-1})$ , (89d) follows  $t = -snr^{-1} s$ , (89d) follows  $z = \mathcal{S}_R(t)$ ,  $\mathcal{R}_R(z) = \mathcal{S}_R^{-1}(-z) - z^{-1}$ ,  $0 = \mathcal{S}_R(-\infty)$  and  $snr v^* = \mathcal{S}_R(snr^{-1} [\rho^* - (v^*)^{-1}])$ , and (89h) follows  $\rho^* = snr \mathcal{R}_R(-snr v^*)$ .

From (88) and (89),  $A_{\text{ADGO}}$  in (43) is consistent with  $C_{\text{LUIS}}(snr)$  in (9). Therefore, we have  $A_{\text{ADGO}} = C_{\text{LUIS}}(snr)$ .

## APPENDIX D

### AN ALTERNATIVE PROOF OF THE CONSTRAINED CAPACITY OF A LUIS

In this appendix, we provide an alternative proof for the constrained capacity of a LUIS using the properties of OAMP. Let  $\hat{\mathbf{x}}_{\text{MMSE}} = \mathbb{E}\{\mathbf{x}|\Gamma, \Phi\}$ . We call  $\mathcal{M}_x(snr) \equiv \frac{1}{N}\mathbb{E}\{\|\mathbf{x} - \hat{\mathbf{x}}_{\text{MMSE}}\|^2\}$  the MMSE of a LUIS and  $\mathcal{M}_{Ax}(snr) \equiv \frac{1}{N}\mathbb{E}\{\|Ax - A\hat{\mathbf{x}}_{\text{MMSE}}\|^2\}$  the measurement MMSE of the LUIS. The following lemma gives the constrained capacity of a LUIS.

*Lemma 11 (Measurement MMSE and Constrained Capacity):* Assume that  $\eta_{\text{SE}}^{-1}(\rho) = \hat{\phi}_{\text{SE}}^S(\rho)$  has a unique positive solution  $\rho^*$ . The measurement MMSE of a LUIS is given by

$$\mathcal{M}_{Ax}(snr) = \rho^* \hat{\phi}_{\text{SE}}^S(\rho^*) / snr = \rho^* \mathcal{M}_x(snr) / snr, \quad (90a)$$

and the constrained capacity is given by

$$C_{\text{LUIS}}(snr) = A_{\text{ADGO}}, \quad (90b)$$

where  $A_{\text{ADGO}}$  is defined in (43).

The next two subsections respectively give the proofs of (90a) and (90b) in Lemma 11.

- In D-A, we prove the measurement MMSE in (90a) of a LUIS using the MMSE optimality [18], [19] and the decoupling property [29] of OAMP.
- In D-B, we prove the constrained capacity in (90b) of a LUIS based on the measurement MMSE in (90a) using the vector-I-MMSE lemma [37].

#### A. Proof of the Measurement MMSE in (90a)

The following proposition is proved for OAMP in [29] (see Theorem 4-A1 in [29]).

*Property 1 (Decoupling):* In OAMP, we define

$$\tilde{\mathbf{z}}_t \equiv \mathbf{x}_t^{\phi \rightarrow \gamma} - \mathbf{x}, \quad (91)$$

Then, the entries of  $\tilde{\mathbf{z}}_t$  are IID with zero mean and variance  $(\hat{\phi}_{\text{SE}}^S(\rho_t)^{-1} - \rho_t)^{-1}$ , and  $\tilde{\mathbf{z}}_t$  can be treated as a random variable that is asymptotically independent<sup>5</sup> with  $\mathbf{n}$  and  $\mathbf{A}$ .

When  $t \rightarrow \infty$ , OAMP converges to a fixed point given by

$$\mathbf{x}_\infty^{\phi \rightarrow \gamma} = \mathbf{x}_*^{\phi \rightarrow \gamma}, \quad \mathbf{x}_\infty^{\gamma \rightarrow \phi} = \mathbf{x}_*^{\gamma \rightarrow \phi}, \quad \rho_\infty = \rho^*. \quad (92)$$

Define  $v_\perp^* = ([\hat{\phi}_{\text{SE}}^S(\rho^*)]^{-1} - \rho^*)^{-1}$ . Then,  $\{\rho^*, v_\perp^*\}$  satisfies the fixed point equations:

$$\rho^* = [\hat{\gamma}_{\text{SE}}(v_\perp^*)]^{-1} - v_\perp^{*-1}, \quad (93a)$$

$$v_\perp^{*-1} = [\hat{\phi}_{\text{SE}}^S(\rho^*)]^{-1} - \rho^*. \quad (93b)$$

In addition,

$$\mathcal{M}_x(snr) = \hat{\gamma}_{\text{SE}}(v_\perp^*) = \hat{\phi}_{\text{SE}}^S(\rho^*). \quad (94)$$

Then, the MMSE estimate of  $\mathbf{x}$  is given by

$$\mathbf{x}_*^{\hat{\gamma}} = \mathbb{E}\{\mathbf{x}|\mathbf{x}_*^{\phi \rightarrow \gamma}, \Gamma\} = [\sigma^{-2} \mathbf{A}^H \mathbf{A} + v_\perp^{*-1} \mathbf{I}]^{-1} [\sigma^{-2} \mathbf{A}^H \mathbf{y} + v_\perp^{*-1} \mathbf{x}_*^{\phi \rightarrow \gamma}]. \quad (95)$$

Note that both  $\mathbf{x}_*^{\hat{\gamma}}$  and  $\mathbf{x}_*^{\hat{\phi}} = \mathbb{E}\{\mathbf{x}|\mathbf{x}_*^{\gamma \rightarrow \phi}, \Phi\}$  are MMSE estimates of  $\mathbf{x}$ , since they have the same MSE (see (94)). Let  $\tilde{\mathbf{z}} = -\tilde{\mathbf{z}}_\infty$ , we then have

$$\mathbf{x} = \mathbf{x}_*^{\phi \rightarrow \gamma} + \tilde{\mathbf{z}}. \quad (96)$$

From Property 1, the entries of  $\tilde{\mathbf{z}}$  are *i.i.d.* with zero mean and variance  $v_\perp^*$ , and  $\tilde{\mathbf{z}}$  behaves independently with  $\mathbf{n}$  and  $\mathbf{A}$ . From (95), (96) and  $\mathbf{y} = \mathbf{A}\mathbf{x} + \mathbf{n}$ , we have

$$\mathbf{x}_*^{\hat{\gamma}} = \mathbf{x} + [\sigma^{-2} \mathbf{A}^H \mathbf{A} + v_\perp^{*-1} \mathbf{I}]^{-1} [\sigma^{-2} \mathbf{A}^H \mathbf{n} + v_\perp^{*-1} \tilde{\mathbf{z}}] \quad (97)$$

From (97), we have

$$\hat{\gamma}_{\text{SE}}(v_\perp^*) = \frac{1}{N} \mathbb{E}\{\|\mathbf{x} - \mathbf{x}_*^{\hat{\gamma}}\|^2\} \quad (98a)$$

$$= \frac{1}{N} \left\| [\sigma^{-2} \mathbf{A}^H \mathbf{A} + v_\perp^{*-1} \mathbf{I}]^{-1} [\sigma^{-2} \mathbf{A}^H \mathbf{n} + v_\perp^{*-1} \tilde{\mathbf{z}}] \right\|^2 \quad (98b)$$

$$= \frac{1}{N} \text{tr} \left\{ [v_\perp^{*-1} \mathbf{I} + \sigma^{-2} \mathbf{A}^H \mathbf{A}]^{-1} \right\}, \quad (98c)$$

<sup>5</sup>Let  $\mathbf{A} = \mathbf{U}\Sigma\mathbf{V}$ . In [29], it is proved that the entries of  $\mathbf{b} = \mathbf{V}\tilde{\mathbf{z}}$  are IIDG and independent with  $\mathbf{n}$  and  $\mathbf{U}\Sigma$ . Based on this, substituting  $\mathbf{A} = \mathbf{U}\Sigma\mathbf{V}$  and  $\mathbf{b} = \mathbf{V}\tilde{\mathbf{z}}$  into (98b), we obtain (98c), which is the same as that  $\tilde{\mathbf{z}}$  is independent with  $\mathbf{n}$  and  $\mathbf{A}$ .

and

$$\mathcal{M}_{Ax}(snr) = \frac{1}{N} \text{E}\{\|\mathbf{A}\mathbf{x} - \mathbf{A}\mathbf{x}_*^\gamma\|^2\} \quad (99a)$$

$$= \frac{1}{N} \text{tr}\left\{\mathbf{A}\left[v_\perp^{*-1}\mathbf{I} + snr\mathbf{A}^H\mathbf{A}\right]^{-1}\mathbf{A}^H\right\} \quad (99b)$$

$$= snr^{-1} - snr^{-1}v_\perp^{*-1}\frac{1}{N} \text{tr}\left\{\left[v_\perp^{*-1}\mathbf{I} + snr\mathbf{A}^H\mathbf{A}\right]^{-1}\right\} \quad (99c)$$

$$= (1 - v_\perp^{*-1}\hat{\gamma}_{\text{SE}}(v_\perp^*))/snr \quad (99d)$$

$$= \rho^* \hat{\phi}_{\text{SE}}^{\mathcal{S}}(\rho^*)/snr, \quad (99e)$$

where (98) follows the assumption that  $\tilde{z}$  behaves independently of  $\mathbf{A}$  and  $\mathbf{n}$ , (99e) follows (98). If OAMP has a unique fixed point, we have  $\mathbf{x}_*^\gamma = \hat{\mathbf{x}}(\mathbf{y}; snr)$  and  $\mathcal{M}_x(snr) = \hat{\gamma}_{\text{SE}}(v_\perp^*) = \hat{\phi}_{\text{SE}}^{\mathcal{S}}(\rho^*)$ . Hence,

$$\mathcal{M}_{Ax}(snr) = (1 - v_\perp^{*-1}\hat{\gamma}_{\text{SE}}(v_\perp^*))/snr = \rho^* \hat{\phi}_{\text{SE}}^{\mathcal{S}}(\rho^*)/snr \quad (100a)$$

$$= [1 - v_\perp^{*-1}\mathcal{M}_x(snr)]/snr = \rho^* \mathcal{M}_x(snr)/snr. \quad (100b)$$

Therefore, we obtain (90a).

### B. Proof of the Constrained Capacity in (90b)

For simplicity, we define

$$\zeta(x) = \frac{1}{N} \text{tr}\{[x\mathbf{A}^H\mathbf{A} + \mathbf{I}]^{-1}\}. \quad (101)$$

We treat  $snr$  as a variable denoted as  $s$ . Then, (93) can be rewritten as

$$\hat{\phi}_{\text{SE}}^{\mathcal{S}}(\rho) = v_\perp \zeta(sv_\perp), \quad \zeta(sv_\perp) = 1/(\rho v_\perp + 1). \quad (102)$$

Let  $z = sv_\perp$ , we have

$$s = z\zeta(z)/\hat{\phi}_{\text{SE}}^{\mathcal{S}}(\rho), \quad \zeta(z) = 1 - \rho\hat{\phi}_{\text{SE}}^{\mathcal{S}}(\rho). \quad (103)$$

Let  $\tilde{s} = s/\rho$  and  $t = \zeta(z) = 1 - \rho\hat{\phi}_{\text{SE}}^{\mathcal{S}}(\rho)$ , we have

$$\tilde{s} = \frac{t}{1-t}\zeta^{-1}(t), \quad (104)$$

where  $\zeta^{-1}(\cdot)$  is inverse of  $\zeta(\cdot)$ .

From the vector I-MMSE lemma and (90a), we have

$$C = \int_0^{snr} \mathcal{M}_{Ax}(s) ds \quad (105a)$$

$$= \int_0^{snr} s^{-1} \rho \hat{\phi}_{\text{SE}}^{\mathcal{S}}(\rho) ds \quad (105b)$$

$$= \int_{s=0}^{s=snr} \tilde{s}^{-1} \hat{\phi}_{\text{SE}}^{\mathcal{S}}(\rho) d(\rho \tilde{s}) \quad (105\text{c})$$

$$= \int_{\rho=0}^{\rho=\rho^*} \tilde{s}^{-1} \hat{\phi}_{\text{SE}}^{\mathcal{S}}(\rho) [\tilde{s} d\rho + \rho d\tilde{s}] \quad (105\text{d})$$

$$= \int_{\rho=0}^{\rho=\rho^*} \hat{\phi}_{\text{SE}}^{\mathcal{S}}(\rho) d\rho + \int_{t=1}^{t=\zeta(snr v_{\perp}^*)} (1-t) d\log \left( \frac{t\zeta^{-1}(t)}{1-t} \right), \quad (105\text{e})$$

where (105c) comes from  $\tilde{s} = s/\rho$ , (105e) from  $\tilde{s} = t\zeta^{-1}(t)/(1-t)$ . Let  $z^* = v_{\perp}^* snr$ , we have

$$\int_{t=1}^{t=\zeta(z^*)} (1-t) d\log \left( \frac{t\zeta^{-1}(t)}{1-t} \right) \quad (106\text{a})$$

$$= \left[ \log(t) \right]_{t=1}^{t=\zeta(z^*)} + \int_{t=1}^{t=\zeta(z^*)} (1-t) d\log(\zeta^{-1}(t)) \quad (106\text{b})$$

$$= \left[ \log(\zeta(z)) + \log(z) \right]_{z=0}^{z^*} - \int_{z=0}^{z^*} \zeta(z)/z dz \quad (106\text{c})$$

$$= \left[ \log(z\zeta(z)) + \frac{1}{N} \log \det(z^{-1} \mathbf{I} + \mathbf{A}^H \mathbf{A}) \right]_{z=0}^{z^*} \quad (106\text{d})$$

$$= \log(z^* \zeta(z^*)) + \frac{1}{N} \log \det(z^{*-1} \mathbf{I} + \mathbf{A}^H \mathbf{A}) \quad (106\text{e})$$

$$= \log(z^* \zeta(z^*)/snr) + \frac{1}{N} \log \det(v_{\perp}^{*-1} \mathbf{I} + snr \mathbf{A}^H \mathbf{A}) \quad (106\text{f})$$

$$= \log \hat{\phi}_{\text{SE}}^{\mathcal{S}}(\rho^*) + \frac{1}{N} \log \det(\mathbf{B}(\rho^*, v^*)) \quad (106\text{g})$$

$$= A_{\text{ADGO}}, \quad (106\text{h})$$

where (106c) comes from  $t = \zeta(z)$ , (106d) from  $\zeta(x) = \frac{1}{N} \text{tr}\{[x \mathbf{A}^H \mathbf{A} + \mathbf{I}]^{-1}\}$  and the law  $\int \text{tr}\{(s \mathbf{I} + \mathbf{A})^{-1}\} ds = \log \det(s \mathbf{I} + \mathbf{A})$ , (106f) from  $z^* = v_{\perp}^* snr$ , and (106g) from  $\hat{\phi}_{\text{SE}}^{\mathcal{S}}(\rho^*) = z^* \zeta(z^*)/snr$ . Thus, we obtain Lemma 11.

## REFERENCES

- [1] E. Biglieri, R. Calderbank, A. Constantinides, A. Goldsmith, A. Paulraj, and H. V. Poor, *MIMO Wireless Communications*. Cambridge, U.K.: Cambridge Univ. Press, 2007.
- [2] Tse David and P. Viswanath, *Fundamentals of wireless communication*. Cambridge university press, 2005.
- [3] L. Liu and W. Yu, “Massive connectivity with massive MIMO—part I: Device activity detection and channel estimation,” *IEEE Trans. Signal Process.*, vol. 66, no. 11, pp. 2933-2946, June 2018.
- [4] L. Liu and W. Yu, “Massive connectivity with massive MIMO—part II: Achievable rate characterization,” *IEEE Trans. Signal Process.*, vol. 66, no. 11, pp. 2947-2959, June 2018.
- [5] D. Micciancio, “The hardness of the closest vector problem with preprocessing,” *IEEE Trans. Inf. Theory*, vol. 47, no. 3, pp. 1212-1215, Mar. 2001.
- [6] S. Verdú, “Optimum multi-user signal detection,” Ph.D. dissertation, Department of Electrical and Computer Engineering, University of Illinois at Urbana-Champaign, Urbana, IL, Aug. 1984.
- [7] S. M. Kay, *Fundamentals of Statistical Signal Processing: Estimation Theory*. Upper Saddle River, NJ, USA: Prentice-Hall, 1993.
- [8] C. Berrou and A. Glavieux, “Near optimum error correcting coding and decoding: Turbo-codes,” *IEEE Trans. Commun.*, vol. 44, no. 10, pp. 1261-1271, Oct. 1996.

- [9] C. Douillard, M. Jézéquel, C. Berrou, D. Electronique, A. Picart, P. Didier, and A. Glavieux, “Iterative correction of intersymbol interference: Turbo-equalization,” *Trans. on Emerging Telecom. Techn.*, vol. 6, no. 5, pp. 507–511, 1995.
- [10] R. G. Gallager, “Low-density parity-check codes,” *IRE Trans. Inform. Theory*, vol. IT-8, pp. 21–28, Jan. 1962.
- [11] S.-Y. Chung, G. D. Forney, Jr., T. J. Richardson, and R. Urbanke, “On the design of low-density parity-check codes within 0.0045 dB of the Shannon limit,” *IEEE Commun. Lett.*, vol. 5, pp. 58–60, Feb. 2001.
- [12] X. Wang and H. V. Poor, “Iterative (Turbo) soft interference cancellation and decoding for coded CDMA,” *IEEE Trans. Commun.*, vol. 47, no. 7, pp. 1046–1061, Jul 1999.
- [13] X. Yuan, L. Ping, C. Xu and A. Kavcic, “Achievable rates of MIMO systems with linear precoding and iterative LMMSE detector,” *IEEE Trans. Inf. Theory*, vol. 60, no. 11, pp. 7073–7089, Oct. 2014.
- [14] L. Liu, C. Yuen, Y. L. Guan, and Y. Li, “Capacity-achieving MIMO-NOMA: iterative LMMSE detection,” *IEEE Trans. Signal Process.*, vol. 67, no. 7, 1758–1773, April 2019.
- [15] Y. Chi, L. Liu, G. Song, C. Yuen, Y. L. Guan and Y. Li, “Practical MIMO-NOMA: low complexity and capacity-approaching solution,” *IEEE Trans. Wireless Commun.*, vol. 17, no. 9, pp. 6251–6264, Sept. 2018.
- [16] G. Reeves and H. D. Pfister, “The replica-symmetric prediction for random linear estimation with Gaussian matrices is exact,” *IEEE Trans. Inf. Theory*, vol. 65, no. 4, pp. 2252–2283, April 2019.
- [17] J. Barbier, N. Macris, M. Dia, and F. Krzakala, “Mutual information and optimality of approximate message-passing in random linear estimation,” *IEEE Trans. Inf. Theory*, vol. 66, no. 7, pp. 4270–4303, July 2020.
- [18] J. Barbier, N. Macris, A. Maillard, F. Krzakala, “The mutual information in random linear estimation beyond i.i.d. matrices,” *arXiv preprint arXiv:1802.08963*, 2018.
- [19] K. Takeda, S. Uda, and Y. Kabashima, “Analysis of cdma systems that are characterized by eigenvalue spectrum,” *EPL (Europhysics Letters)*, vol. 76, no. 6, p. 1193, 2006.
- [20] L. Liu, C. Liang, J. Ma, and L. Ping, “Capacity optimality of AMP in coded linear systems”, *IEEE Trans. Inf. Theory*, vol. 67, no. 7, 4929–4445, July 2021
- [21] D. L. Donoho, A. Maleki, and A. Montanari, “Message-passing algorithms for compressed sensing,” in *Proc. Nat. Acad. Sci.*, vol. 106, no. 45, Nov. 2009.
- [22] M. Bayati and A. Montanari, “The dynamics of message passing on dense graphs, with applications to compressed sensing,” *IEEE Trans. Inf. Theory*, vol. 57, no. 2, pp. 764–785, Feb. 2011.
- [23] J. Ma and L. Ping, “Orthogonal AMP,” *IEEE Access*, vol. 5, pp. 2020–2033, 2017, preprint arXiv:1602.06509, 2016.
- [24] J. Ma, X. Yuan and L. Ping, “Turbo compressed sensing with partial DFT sensing matrix,” *IEEE Signal Process. Lett.*, vol. 22, no. 2, pp. 158–161, Feb. 2015.
- [25] J. Ma, X. Yuan and L. Ping, “On the performance of Turbo signal recovery with partial DFT sensing matrices,” *IEEE Signal Process. Lett.*, vol. 22, no. 10, pp. 1580–1584, Oct. 2015.
- [26] F. Hiai and D. Petz, *The Semicircle Law, Free Random Variables and Entropy*. Amer. Math. Soc., 2000.
- [27] A. M. Tulino and S. Verdú, “Random matrix theory and wireless communications.” *Commun. and Inf. theory*, 2004.
- [28] S. Rangan, P. Schniter, and A. Fletcher, “Vector approximate message passing,” *IEEE Trans. Inf. Theory*, vol. 65, no. 10, pp. 6664–6684, Oct. 2019.
- [29] K. Takeuchi, “Rigorous dynamics of expectation-propagation-based signal recovery from unitarily invariant measurements,” *IEEE Trans. Inf. Theory*, vol. 66, no. 1, 368 - 386, Jan. 2020.
- [30] K. Takeuchi, “Bayes-optimal convolutional AMP,” *IEEE Trans. Inf. Theory*, vol. 67, no. 7, pp. 4405–4428, July 2021.
- [31] L. Liu, S. Huang, and B. M. Kurkoski, “Memory approximate message passing,” *Proc. 2021 IEEE Int. Symp. Inf. Theory*, pp.1379-1384, Melbourne, Australia, July 2021, arXiv preprint arXiv:2012.10861, Dec. 2020.
- [32] J. Ma, L. Liu, X. Yuan and L. Ping, ”On orthogonal AMP in coded linear vector systems,” *IEEE Trans. Wireless Commun.*, vol. 18, no. 12, pp. 5658–5672, Dec. 2019.
- [33] M. Khani, M. Alizadeh, J. Hoydis and P. Fleming, “Adaptive neural signal detection for massive MIMO,” *IEEE Trans. Wireless Commun.*, vol. 19, no. 8, pp. 5635–5648, Aug. 2020,
- [34] J. Zhang, H. He, C. Wen, S. Jin and G. Y. Li, “Deep learning based on orthogonal approximate message passing for CP-Free OFDM,” *IEEE International Conference on Acoustics, Speech and Signal Processing (ICASSP)*, 2019, pp. 8414–8418,

- [35] Y. Cheng, M. A. Van Wyk and L. Ping, "Orthogonal AMP Detection Techniques for Massive Access over OFDM," *IEEE Commun. Lett.*, 2021. (Early access)
- [36] Y. Cheng, L. Liu and L. Ping, "Orthogonal AMP for massive access in channels with spatial and temporal correlations" *IEEE J. Sel. Areas Commun.*, vol. 39, no. 3, 726-740, March 2021.
- [37] D. Guo, S. Shamai, and S. Verdú, "Mutual information and minimum mean-square error in Gaussian channels," *IEEE Trans. Inf. Theory*, vol. 51, no. 4, pp. 1261-1282, Apr. 2005.
- [38] K. Bhattacharjee and K. R. Narayanan, "An MSE-based transfer chart for analyzing iterative decoding schemes using a Gaussian approximation," *IEEE Trans. Inf. Theory*, vol. 53, no. 1, pp. 22-38, Jan. 2007.
- [39] Y. Cheng, L. Liu, L. Ping, "An Integral-Based Approach to Orthogonal AMP," *IEEE Signal Process. Lett.*, vol. 28, 194-198, Dec. 2020.
- [40] T. P. Minka, "Expectation propagation for approximate bayesian inference," in *Proceedings of the Seventeenth conference on Uncertainty in artificial intelligence*, 2001, pp. 362-369.
- [41] M. Opper and O. Winther, "Expectation consistent approximate inference," *Journal of Machine Learning Research*, vol. 6, no. Dec, pp. 2177-2204, 2005.
- [42] B. Çakmak and M. Opper, "Expectation propagation for approximate inference: Free probability framework," *arXiv preprint arXiv:1801.05411*, 2018.
- [43] E. Schmidt, "Über die auflösung linearer gleichungen mit unendlich vielen unbekannten," *Rend. Circ. Mat. Palermo* (1884-1940), vol. 25, no. 1, 53-77, 1908.
- [44] C. Stein, "A bound for the error in the normal approximation to the distribution," in *Proc. 6th Berkeley Symp. Math. Statist. Probab.*, 1972.
- [45] S. Campese, "Fourth moment theorems for complex Gaussian approximation," 2015, arXiv:1511.00547.
- [46] R. Y. S. Tee, R. G. Maunder and L. Hanzo, "EXIT-chart aided near-capacity irregular bit-interleaved coded modulation design," *IEEE Trans. Wireless Commun.*, vol. 8, no. 1, pp. 32-37, Jan. 2009.
- [47] L. Kong, S. X. Ng, R. Y. S. Tee, R. G. Maunder and L. Hanzo, "Reduced-complexity near-capacity downlink iteratively decoded generalized multi-layer space-time coding using irregular convolutional codes", *IEEE Trans. Wireless Commun.*, vol. 9, no. 2, pp. 684-695, Feb. 2010.
- [48] K. Wu, K. Anwar, T. Matsumoto, "BICM-ID-based IDMA: Convergence and rate region analyses," *IEICE Trans. Commun.*, vol. E97.B, no. 7, pp. 1483-1492, July 2014.
- [49] D. Guo and S. Verdú, "Randomly spread CDMA: Asymptotics via statistical physics," *IEEE Trans. Inf. Theory*, vol. 51, no. 6, pp. 1983-2010, Jun. 2005.
- [50] T. Tanaka, "A statistical-mechanics approach to large-system analysis of CDMA multiuser detectors," *IEEE Trans. Inf. Theory*, vol. 48, no. 11, pp. 2888-2910, Nov. 2002.
- [51] J. Vila, P. Schniter, S. Rangan, F. Krzakala, and L. Zdeborová, "Adaptive damping and mean removal for the generalized approximate message passing algorithm," in *Acoustics, Speech and Signal Processing (ICASSP), 2015 IEEE International Conference on*, 2015, pp. 2021-2025.
- [52] X. Yuan, *Low-complexity iterative detection in coded linear systems*, PhD thesis, City University of Hong Kong, Hong Kong, China, 2008.
- [53] S.-Y. Chung, T. Richardson, and R. Urbanke, "Analysis of sum-product decoding of low-density parity-check codes using a Gaussian approximation," vol. 47, no. 2, pp. 657-670, Feb. 2001.
- [54] D. Williams, *Probability with martingales*, Cambridge Univ. Press, 2001.
- [55] A. Lozano, A. M. Tulino and S. Verdú, "Optimum power allocation for parallel Gaussian channels with arbitrary input distributions," *IEEE Trans. Inf. Theory*, vol. 52, no. 7, pp. 3033-3051, July 2006.
- [56] R. Berthier, A. Montanari, P. M. Nguyen, "State evolution for approximate message passing with non-separable functions," *Information and Inference: A Journal of the IMA*, vol. 9, no. 1, pp. 33-79, Mar. 2020.